Article

Magmatic Evolution and Rare Metal Mineralization in Mount El-Sibai Peralkaline Granites, Central Eastern Desert, Egypt: Insights from Whole-Rock Geochemistry and Mineral Chemistry Data

Mabrouk Sami [1,]*[ ], Hassan Osman [1,]*, Awaad F. Ahmed [1], Khairy S. Zaky [1], Rainer Abart [2], Ioan V. Sanislav [3], Kamal Abdelrahman [4][ ], Mohammed S. Fnais [4], Wenzhou Xiao [5,6] and Hassan Abbas [7][ ]

[1] Geology Department, Faculty of Science, Minia University, El-Minia 61519, Egypt; awaadahmed58@mu.edu.eg (A.F.A.); khairy.abdelmegeed@mu.edu.eg (K.S.Z.)
[2] Department of Lithospheric Research, University of Vienna, Althanstrasse 14, A-1090 Vienna, Austria; rainer.abart@univie.ac.at
[3] Economic Geology Research Centre (EGRU), College of Science and Engineering, James Cook University, Townsville, QLD 4811, Australia; ioan.sanislav@jcu.edu.au
[4] Department of Geology & Geophysics, College of Science, King Saud University, P.O. Box 2455, Riyadh 11451, Saudi Arabia; khassanein@ksu.edu.sa (K.A.); mfnais@ksu.edu.sa (M.S.F.)
[5] Hunan Key Laboratory of Rare Metal Minerals Exploitation and Geological Disposal of Wastes, School of Resource Environment and Safety Engineering, University of South China, Hengyang 421001, China; lilzhou@usc.edu.cn
[6] Fundamental Science on Radioactive Geology and Exploration Technology Laboratory, East China University of Technology, Nanchang 330013, China
[7] Geology Department, Faculty of Science, Assiut University, Assiut 71526, Egypt; hassanabbas@science.aun.edu.eg
[*] Correspondence: mabrouk.hassan@mu.edu.eg (M.S.); hassanosman@mu.edu.eg (H.O.)

Abstract: The Ediacaran peralkaline granites, which were emplaced during the post-collisional tectonic extensional stage, have a limited occurrence in the northern tip of the Nubian Shield. In this contribution, we present new mineralogical and geochemical data of Mount El-Sibai granites from the Central Eastern Desert of Egypt. The aim is to discuss their crystallization condition, tectonic setting, and petrogenesis as well as the magmatic evolution of their associated mineralization. Mount El-Sibai consists of alkali-feldspar granites (AFGs) as a main rock unit with scattered and small occurrences of alkali-amphibole granites (AAGs) at the periphery. The AAG contain columbite, nioboaeschynite, zircon and thorite as important rare metal-bearing minerals. Geochemically, both of AFG and AAG exhibit a highly evolved nature with a typical peralkaline composition (A/CNK = 0.82–0.97) and formed in within-plate anorogenic setting associated with crustal extension and/or rifting. They are enriched in some LILEs (Rb, K, and Th) and HFSEs (Ta, Pb, Zr, and Y), but strongly depleted in Ba, Sr, P and Ti with pronounced negative Eu anomalies (Eu/Eu* = 0.07–0.34), consistent with an A-type granite geochemical signature. The calculated T_{Zrn} (774–878 °C) temperatures indicate that the magma was significantly hot, promoting the saturation of zircon. The texture and chemistry of minerals suggest that they were crystallized directly from a granitic magma and were later subject to late- to post-magmatic fluids. Both granitic types were most likely generated through partial melting of a juvenile crustal source followed by magmatic fractionation. The lithospheric delamination is the main mechanism which causes uplifting of the asthenospheric melts and hence provides enough heat for crustal melting. The produced parent magma was subjected to prolonged fractional crystallization to produce the different types of Mount El-Sibai granites at different shallow crustal levels. During magma fractionation, the post-magmatic fluids (especially fluorine) contribute significantly to the formation of rare metal mineralization within Mount El-Sibai granites.

Keywords: fractional crystallization; rare metals; peralkaline granite; columbite; Mount El-Sibai; Nubian Shield

1. Introduction

Peralkaline A-type magmatic rocks are frequently found in multiphase intrusions within intracontinental extensional settings, and their mineral compositions can vary widely [1,2]. These rocks contain significant amounts of alkali metals ($Na_2O + K_2O/Al_2O_3 > 1$) and incompatible elements, such as Zr, Hf, Nb, and Ta. They are sourced from multiple origins and undergo various processes and tectonic settings that contribute to their diverse mineral and geochemical contents [3,4]. Peralkaline granites have attracted considerable attention from researchers due to their potential as indicators of magmatic processes, formation conditions and tectonic environments. The Neoproterozoic alkaline/peralkaline granites are widely distributed in the Arabian Nubian Shield (ANS) (Figure 1a), but their precise origin is still a topic of debate [3].
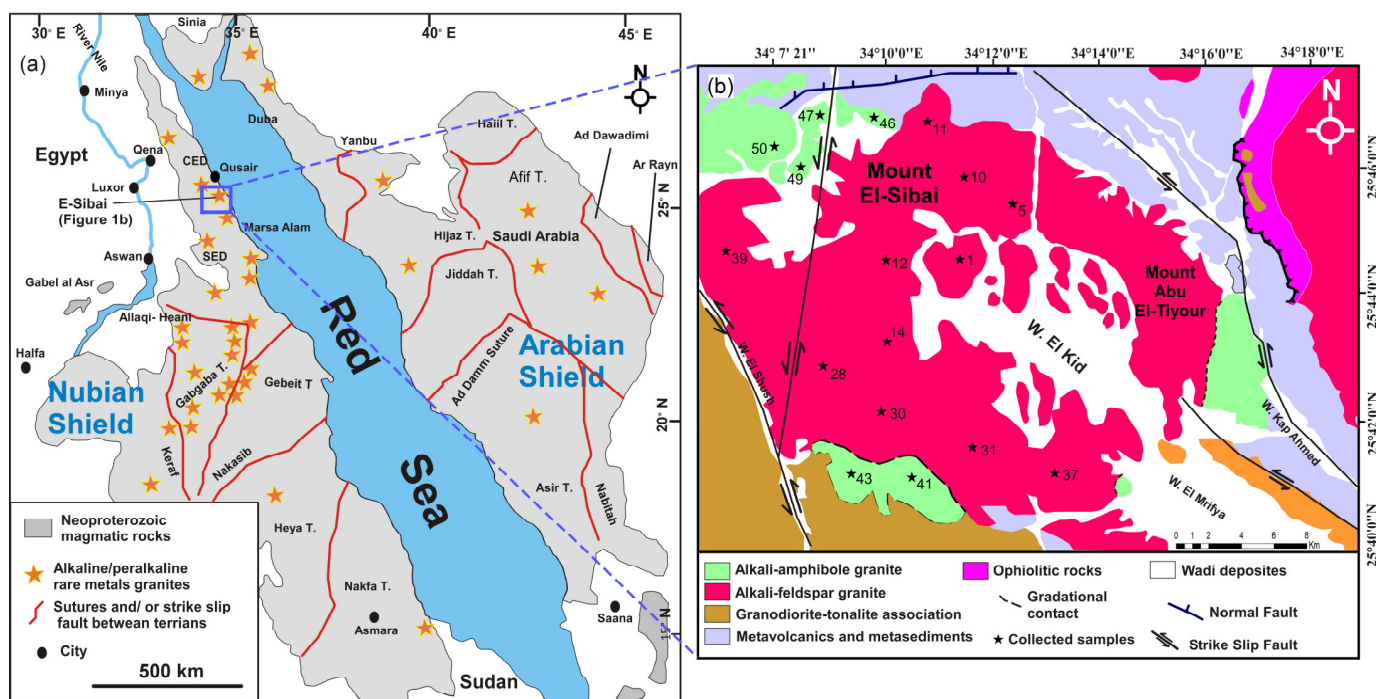
Figure 1. (**a**) General geologic map of the ANS, showing the distribution of the alkaline/peralkaline granitic plutons including the location of the study area; (**b**) geologic map of Mount El-Sibai area showing the distribution of the analyzed samples.

The basement rocks found in the Eastern Desert are the northernmost exposures of the ANS and were formed during the late Proterozoic Pan-African events (900–550 Ma) [5–7]. These rocks are made up of a juvenile crust that was created by the merging and accumulation of continental and oceanic magmatic arcs [7,8]. In the ANS's northern region, many granitoids were formed during the syn-orogenic and late-to-post-orogenic stages. Subduction and collision events caused the development of syn-orogenic calc-alkaline magmatism, followed by post-collisional magmatism that generated high-K calc-alkaline, alkaline, and peralkaline rocks in the final stages of the Pan-African orogeny (650–550 Ma) [7,9,10]. The alkaline/peralkaline granites from the Egyptian Eastern Desert are currently attracting considerable attention because they frequently contain appreciated concentrations of rare earth elements (REEs), U, Th, Ta, and Nb, which are of potential economic value [5,11]. Despite numerous studies on post-collisional peralkaline granites in the Egypt Eastern Desert, their origin and geotectonic evolution remain uncertain [12].

Mount El-Sibai (640–590 Ma; [13]), situated in the central Eastern Desert of Egypt (Figure 1b), is a significant peralkaline intrusion. Previous studies have examined the petrological and isotopic characteristics of El-Sibai granites [13–16]. However, the origin of these

specialized geochemical peralkaline granites and their associated rare metal mineralization remains a topic of contention. Therefore, this article provides new fieldwork observations, and whole-rock (major and trace elements) geochemical and in situ mineral chemistry data of the Mount El-Sibai granites. The main objective is to provides insights into the tectonic setting and magmatic evolution of the studied granites, along with explaining the mechanisms by which the rare metal-bearing minerals (e.g., fluorite, columbite, thorite, zircon, and nioboaeschynite) were formed within El-Sibai granites.

2. Geologic Setting

The ANS is a prominent Pan-African orogenic belt that extends across accreted terranes from the Mozambique and Madagascar belts in the east to Eastern Egypt, Sinai, Jordan, Western Arabia, and Yemen in the west [8,17] (Figure 1a). The juvenile crust of the ANS was formed during the Neoproterozoic Era through a pre-collisional stage characterized by island-arc volcanism [8]. The collisional stage ended between 615 and 600 Ma, followed by orogenic collapse within the period 595–575 Ma, and subsequent transpressional tectonism along significant shear zones [18–20]. After the cessation of the Pan-African orogenic compressive tectonic activity around 550 Ma, an extended phase of anorogenic alkaline complexes intruded over almost the entire Phanerozoic Era until the opening of the Red Sea about 23 Ma ago [3,21]. These alkaline complexes primarily intruded along deep-seated, reactivated, Pan-African fractures and shear zones, or at the intersections of such fracture systems. Many of these occurrences are associated with significant mineralization and hydrothermal alteration [22].

In the Egyptian basement complex, granitoids are the most dominant intrusive rocks, making up about 50% of all such rocks [23,24]. These granitoids are traditionally categorized into two main groups based on their age, composition, and geochemistry. The older suite is characterized as grey, calc-alkaline, syn-tectonic, I-type intrusions, ranging in composition from diorite to granodiorite, and occasionally granite. The younger suite, on the other hand, comprises, typically pink to red, calc-alkaline, alkaline and peralkaline, late to post-tectonic, I- and A-type granites [25].

The Mount El-Sibai granitic pluton is a prominent mountainous region (~1378 m; as a maximum altitude) situated in the central Eastern Desert of Egypt, between latitudes 25°47′ N and 25°40′ N, and longitudes 34°04′ E and 34°16′ E (Figure 1b). The pluton consists of medium- to very coarse-grained, massive, white grey to pink alkaline granitic rocks. It crosscuts host rocks composed of tonalite, granodiorite, metasedimentary, and metavolcanic rocks, displaying sharp and nonreactive contacts. Field and petrographic investigations indicate that Mount El-Sibai constitutes a composite pluton with two major units. The main unit, which makes up approximately 95% of the pluton, primarily consists of alkali-feldspar granites (AFGs) with small occurrences of alkali-amphibole-bearing granites (AAGs) located at the northern and southern ends, respectively (Figure 1b). The AFGs are massive, medium- to coarse-grained, and typically have red-gray to reddish-pink colors, although they appear monotonous in the field. Additionally, the AFGs are extensively deformed within the pluton's core. The AAGs have gradational contacts with AFGs (Figure 2a) and sharp contacts with metavolcanic and metasedimentary rocks without any evidence of meta-somatic alteration (Figure 2b). The AAGs are medium-grained and exhibit a range of pink, rose, and reddish colors, although they share the same petrographic characteristics. The eastern portion of the mapped area is characterized by low-moderate hills with gentle slopes, where granodiorites are exposed. These granodiorites are gray, medium- to coarse-grained rocks that are rich in mafic minerals. Two sets of NW- and N-trending quartz veins and doleritic to trachytic dykes cross-cut Mount El-Sibai.

Figure 2. (**a**) Field photograph showing the sharp contact between the main granitic varieties (AFG and AAG) of Mount El-Sibai; (**b**) field photograph displaying the sharp contact between AAG and metavolcanics in the north of Mount El-Sibai.

3. Analytical Methods

The complete description of the analytical methods is provided in the Supplementary Document S1. Here, we mention the methods used in this study. Thirty-six refined polished thin sections were prepared for mineralogical and petrographic studies using optical polarizing microscope at the Geology Department, Assuit University (Egypt). A subset of these sections was selected and coated with carbon for the analysis of major minerals (K-feldspar, plagioclase, amphibole, and biotite) and ore minerals (zircon, thorite, columbite, and nioboaeschynite) using a CAMECA SX5 electron microprobe (CAMECA, Gennevilliers Cedex, France) at the Department of Lithospheric Research, University of Vienna (Austria). A total of 20 representative samples were selected for whole-rock major, trace, and REEs analyses using a sequential Philips PW 2400 X-ray spectrometer (Malvern Panalytical, Malvern, United Kingdom) at University of Vienna (Austria) and Laser Ablation ICP-MS at Central Analytical Facilities Lab, Stellenbosch University (South Africa).

4. Results

4.1. Petrographic Features and Mineral Chemistry

Petrographic examination supports the division of the investigated granites into alkali-feldspar granites (AFGs) and alkali-amphibole bearing granites (AAGs). The AFGs are typically characterized by a pink to pale pink color, medium-to-coarse-grained (Figure 3a), and a hypidiomorphic texture (Figure 3b). They primarily consist of alkali feldspars (45–63%) and quartz (29–36%), along with varying amounts of plagioclase (2–5%) and mafic minerals (1–2%). Accessory minerals (>1 vol%) such as zircon, rutile, ilmenite, and magnetite are also present. The most common feldspar is perthite, but microcline and albite can also be present (Figure 3b,c). Perthite displays various patterns, including veined, flame, and patchy, and may contain small quartz crystals. Quartz can be found as interstitial anhedral crystals and as fine, irregular grains that form micrographic intergrowths. In samples from the pluton's core, quartz exhibits undulatory extinction due to deformations. Plagioclase occurs as fresh prismatic and tabular crystals, while biotite is the only mafic mineral present and appears as subhedral ragged flakes.
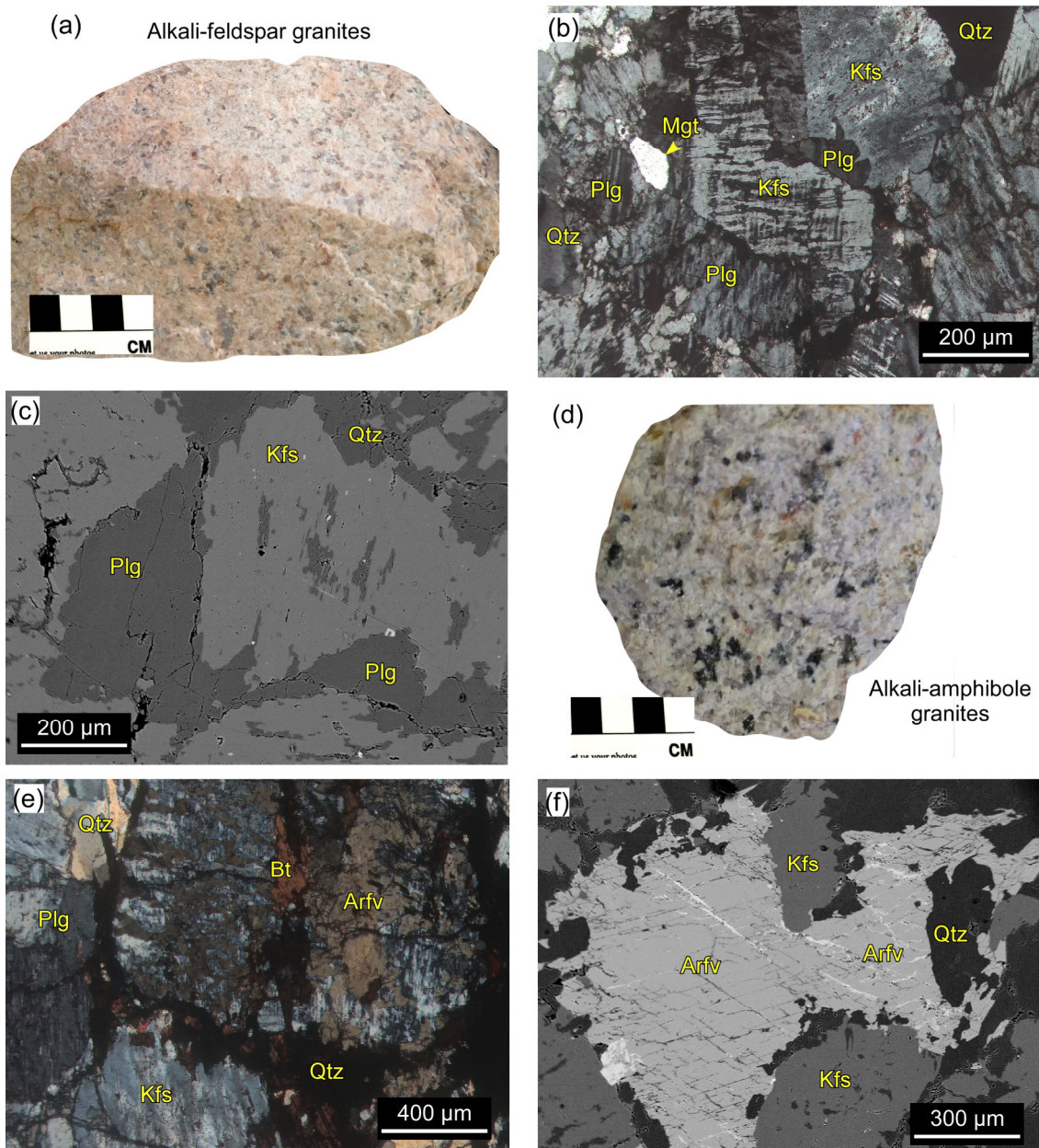
Figure 3. (**a**) Hand specimen shows the main pink to pale pink appearance of AFGs; (**b**) photomicrograph (XPL) showing the hypidiomorphic texture of AFGs; (**c**) back-scattered electron images (BSE) showing the occurrence of plagioclase (Plg), K-feldspar (Kfs), and quartz (Qtz) as the main mineral association of AFGs; (**d**) hand specimen exhibit the main reddish to pale grey appearance of AAGs; (**e**) photomicrograph (XPL) displaying the intergrowth of biotite (Bt), arfvedsonite (Arfv) in AAGs with a typical hypidiomorphic texture; (**f**) BSE images of a well-developed subhedral coarse grained a arfvedsonite (Arfv) crystal within AAGs.

The AFGs and AAGs are almost identical, with the primary distinguishing feature being the higher abundance of alkali-amphiboles in the AAGs. The AAGs are medium to coarse-grained with a hypersolvus and hypidiomorphic granular texture (Figure 3d). They consist of K-feldspars (41–56%), quartz (24–33%), plagioclase (2–8%), alkali-amphibole (2–3%) and biotite (0.5–1%) (Figure 3e). Accessory minerals present include magnetite, ilmenite, zircon, columbite, thorite, nioboaeschynite, and fluorite. The K-feldspars in the AAGs include orthoclase perthite and microcline, and perthitic crystals can display flame, patchy, and vein–perthitic intergrowth types. Quartz occurs as anhedral to euhedral

interstitial crystals or as micrographic intergrowths with K-feldspars, and some quartz crystals contain small inclusions of mafic minerals and feldspars. Plagioclase is represented only by albite, occurring as subhedral laths or as inclusions in perthite and quartz crystals. The mafic minerals in the AAG consist mainly of sodic amphibole and biotite, occurring as subhedral to anhedral crystals interstitial to the essential minerals (Figure 3e,f). Zircon and thorite occur as clear euhedral isolated crystals or as inclusions in the mafic minerals. A few well-formed crystals of columbite and nioboaeschynite are found to be associated with Fe-Ti oxides, while discrete fluorite crystals are observed to be filling the interstitial spaces between other minerals.

Representative microprobe analyses (EPMA) of the major silicates and rare metal-bearing minerals from the examined rocks are provided in Supplementary Tables S1–S8.

4.1.1. Feldspars

The chemical compositions of representative K-feldspars and plagioclase crystals are provided in Supplementary Tables S1 and S2 and are illustrated in Figure 4a. The K-feldspar content is represented by Or_{97-99} in AFGs and Or_{97-98} in AAGs, with high K_2O contents (16.21–16.64 wt.% in AFGs and 16.22–16.56 wt.% in AAGs). The concentration of CaO in all the analyzed K-feldspar crystals is low, with a maximum value of 0.04 wt.%. Plagioclase in both granitic varieties consist of pure albite compositions (AFG-$Ab_{0-0.33}$ and AAG-$An_{0-0.11}$). Albite has Na_2O contents ranging from 11.58 to 12.00 wt.% in AFGs and is tightly restricted between 11.77 and 12.06 wt.% in AAGs. The CaO content in albite is less than 0.07 wt.%.
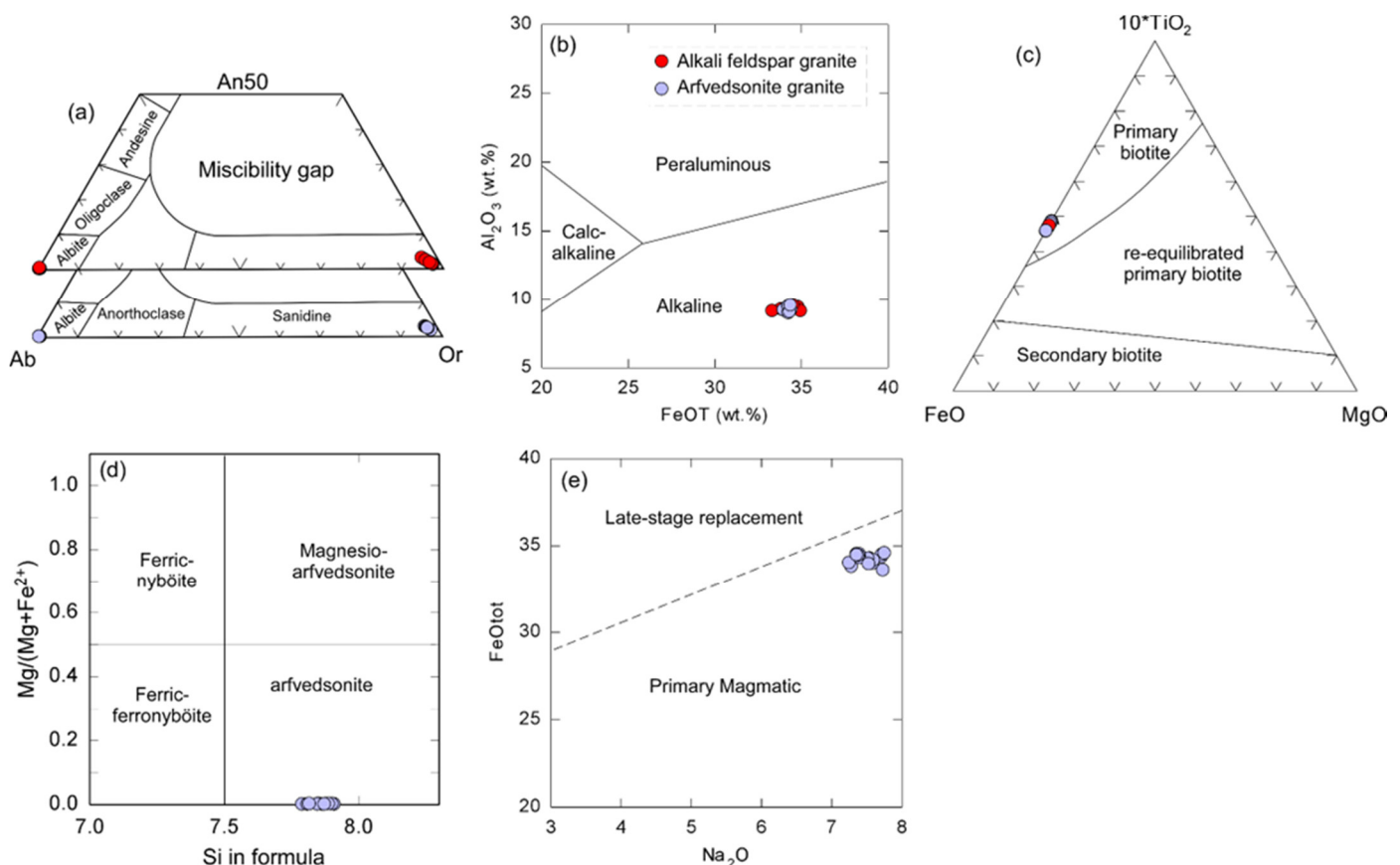
Figure 4. (**a**) Feldspars composition of Mount El-Sibai granites plotted in the An-Ab-Or diagram (data in mol.%); (**b**) Al_2O_3-FeO^t diagram for the biotite [26]; (**c**) 10 * TiO_2-(FeO + MnO)-MgO ternary diagram discriminating between primary, re-equilibrated, and secondary biotite [27]; (**d**) classification of the sodic amphiboles as per IMA norm [28], and (**e**) Na_2O vs. FeO diagram discriminating between primary and late-stage replacement of amphiboles [29].

4.1.2. Biotite

Biotite is recorded in both granitic varieties with quite similar chemical composition. The representative EMPA analyses are provided in Supplementary Table S3. In general, biotite in both rock types has relatively high concentrations of FeO^t (33.33–34.97 wt.%) and TiO_2 (2.88–3.23 wt.%), and low contents of Al_2O_3 (8.96–9.52 wt.%) and MnO (0.35–0.55 wt.%). It is classified as Fe-biotite and falls within the alkaline granitic field, with a typical magmatic origin (Figure 4b,c).

4.1.3. Amphibole

Amphibole is the predominant mafic mineral in the AAG. Representative EMPA analyses are provided in Supplementary Table S4. It is classified as a Na-amphibole with arfvedsonite composition (Figure 4d). All the analyzed grains contain high FeO^t (33.59–34.56 wt.%) and Na_2O (7.26–7.76 wt.%), which are characteristic of primary igneous amphiboles (Figure 4e).

4.1.4. Zircon ($ZrSiO_4$) and Thorite ($ThSiO_4$)

Representative EMPA analyses of zircon and thorite are presented in Supplementary Table S5. In comparison to AFG, zircon from the AAG occasionally contains or is intergrown with thorite (Figure 5a). Thorite is also intergrown or hosted by fluorite (Figure 5b). Both types of granites exhibit almost similar zircon chemical compositions, with ZrO_2 ranging from 61.10 to 65.47 wt.% and HfO_2 ranging from 1.60 to 4.88 wt.%. The ThO_2/UO_2 ratio ranges from 0.2 to 2.4), typical of magmatic zircons [30] (Figure 6a). Thorite crystals exhibit large variations in chemical composition [ThO_2 (61.38–69.71 wt.%), UO_2 (2.45–9.24 wt.%) and Y_2O_3 (3.29–5.14 wt.%)].
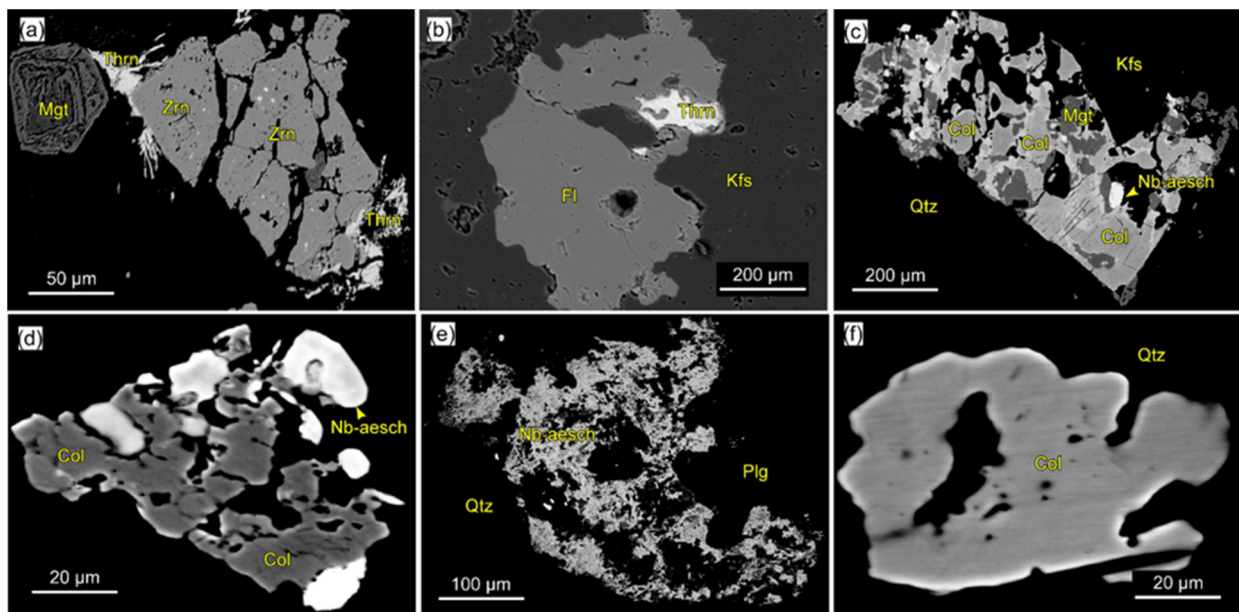
Figure 5. Back-scattered electron (BSE) images showing (**a**) the intergrown of zircon (Zrn), thorite (Thrn) and magnetite (Mgt); (**b**) thorite partially hosted by fluorite (Fl) and K-feldspar (Kfs) in AAGs; (**c**) aggregation of columbite (Col), nioboaeschynite (Nb-aesch) and magnetite (Mgt) between quartz (Qtz) and K-feldspar; (**d**) columbite intergrowth surrounded by nioboaeschynite crystals; (**e**) nioboaeschynite crystallized between quartz and plagioclase (Plg) and (**f**) clear subhedral columbite hosted by quartz in AAGs.
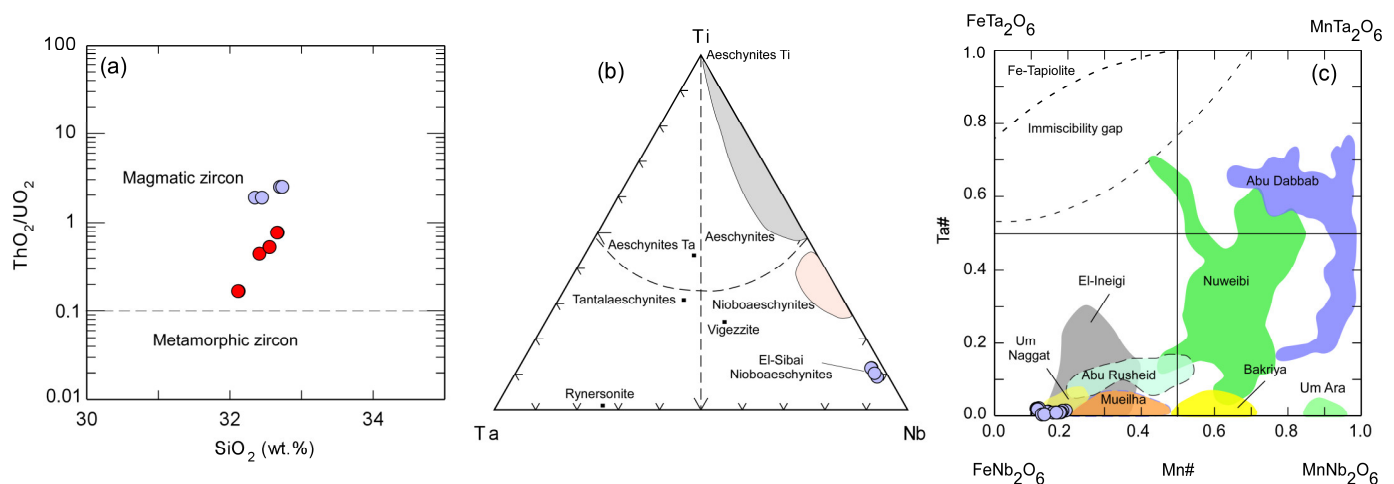
Figure 6. (**a**) Composition of zircon plotting on ThO_2/UO_2 vs. SiO_2 diagram, which discriminates between magmatic and metamorphic zircon; (**b**) plotting of Mount El-Sibai nioboaeschynite composition on the Ti-Nb-Ta ternary diagram for the aeschynite group minerals (after Deliens, [31]); and (**c**) plotting Plot of Ta/(Ta + Nb) vs. Mn/(Mn + Fe) ratios of columbite group minerals from Mount El-Sibai AAGs in comparison with other rare metal-bearing granites from the Eastern Desert of Egypt (after Sami et al., [32]). Symbol as in Figure 4.

4.1.5. Fluorite

Fluorite occurs as subhedral crystals in AAGs, often intergrown with thorite and other REE-bearing phases such as nioboaeschynite (Figure 5b). It has an F compositional range from 46.38 to 47.91% (Supplementary Table S6).

4.1.6. Nioboaeschynite-(Ce)

Nioboaeschynite is newly discovered in peralkaline granites from the Egyptian Eastern Desert in general, and specifically in the El-Sibai AAG. It normally occurs as intergrown crystals with columbite (Figure 5c,d) or as independent crystals between the major mineral phases such as quartz and plagioclase (Figure 5e).

The representative EMPA analyses of nioboaeschynite are presented in Supplementary Table S7 and Figure 6b. Niobium (Nb_2O_5 = 60.27–64.87 wt.%) and Ce (Ce_2O_3 = 17.26–22.15 wt.%) are the main constituents (Figure 6b). Other important oxides are TiO_2 (3.96–5.0 wt.%), CaO (3.03–4.38 wt.%) and Ta_2O_3 (3.29–3.38 wt.%). Therefore, it is classified as nioboaeschynite-Ce.

4.1.7. Columbite-(Fe)

Columbite is the main Nb-oxide in the orthorhombic columbite–tantalite group minerals (CGMs) which is usually found in rare-metal granites and pegmatites, but this mineral is also common in F- and Li-rich peraluminous granitic systems and associated greisens [33]. The occurrence of CGM has attracted significant attention because they are minerals of economic interest hosted in several metallogenetic provinces worldwide [5].

Columbite (for representative chemical analyses see Supplementary Table S8) is the main Nb-Ta bearing phase in AAGs. It occurs in aggregation with nioboaeschynite (Figure 5c,d) and/or as subhedral independent crystals between the main mineral phases (Figure 5f). Columbite analyses are plotted together with other CGMs from different localities in the Egyptian Eastern Desert in the Mn/(Fe + Mn) (Mn#) vs. Ta/(Nb + Ta) (Ta#) diagram (Figure 6c). The analyzed columbite occupy the left quarter of the quadrilateral diagram, with low Mn# (0.11–0.19) and Ta# (>0.02) and are thus classified as columbite-(Fe). It is worth noting that the columbite-(Fe) crystals from Mount El-Sibai AAGs display low Ta/(Ta + Nb) ratios (up to 0.02) compared to those of similar columbite-(Fe) composition

found in El-Ineigi and Abu Rushied [32], which are post-orogenic granitic plutons in the Eastern Desert of Egypt (Figure 6c).

4.2. Whole-Rock Geochemical Characteristics

The chemical analyses of the studied samples and their calculated normative mineral compositions are listed in Tables 1 and 2. These samples exhibit a highly evolved nature, with SiO_2 content ranging from 76.34% to 78.74% wt.%, and a high abundance of total alkalis ($Na_2O + K_2O$ = 8.29–9.78 wt.%). From the R1–R2 diagram (Figure 7a), the analyzed samples are categorized within the alkali granite field. Using the $FeO^t/(FeO^t + MgO)$ vs. SiO_2 relation [34], the AFGs and AAGs strictly fit well in the ferroan field (Figure 7b). Moreover, the studied granites fall within the alkaline field in the diagram of Sylvester [35] (Figure 7c). The peralkaline nature of the El-Sibai granites is confirmed by their molar $Al_2O_3/Na_2O + K_2O > 1$ value (Figure 7d).

Table 1. Whole-rock geochemical analysis of major (wt.%) and trace (ppm) elements of Mount El-Sibai granites.

Rock Type	Alkali-Feldspar Granites											Alkali-Amphibole-Bearing Granites					
No.	SG1	SG5	SG10	SG11	SG12	SG14	SG28	SG30	SG31	SG37	SG39	SG41	SG43	SG46	SG47	SG49	SG50
SiO_2	78.62	76.53	77.2	77.37	76.91	78.14	78.74	77.83	77.28	76.54	76.48	76.34	77.46	77.37	76.98	77.34	77.13
TiO_2	0.06	0.08	0.06	0.06	0.06	0.06	0.04	0.06	0.05	0.09	0.08	0.06	0.04	0.05	0.06	0.07	0.05
Al_2O_3	11.16	11.65	12.22	11.94	11.61	11.79	11.46	11.56	11.5	11.34	11.94	11.37	11.19	11.34	11.54	12.09	11.54
Fe_2O_3	1.64	1.6	0.89	1.53	1.55	1.23	1.27	1.11	1.23	1.62	1.59	1.72	1.4	0.93	1.48	1.16	1.53
MnO	0.02	0.03	0.02	0.01	0.02	0.01	0.01	0.01	0.02	0.02	0.02	0.01	0.02	0.01	0.01	0.01	0.01
MgO	0.02	0.02	0.03	0.02	0.06	0.01	0.03	0.07	0.08	0.02	0.09	0.02	0.02	0.04	0.03	0.05	0.03
CaO	0.25	0.34	0.3	0.25	0.22	0.25	0.14	0.26	0.37	0.36	0.57	0.32	0.28	0.27	0.42	0.21	0.4
Na_2O	4.31	4.48	4.68	4.47	4.64	4.64	4.5	4.64	4.27	4.92	4.8	5.15	4.79	4.98	4.46	4.49	4.46
K_2O	4	4.53	4.23	4.55	4.17	3.99	3.84	3.65	4.27	4.5	4.31	4.22	4.01	4.8	4.42	4.45	4.41
P_2O_5	0.01	0.02	0.01	0.02	0.04	0.01	0.01	0.02	0.03	0.04	0.04	0.01	0.02	0.01	0.02	0.01	0.01
LOI	0.32	0.32	0.18	0.16	0.35	0.19	0.11	0.39	0.39	0.6	0.67	0.21	0.42	0.26	0.27	0.42	0.22
Total	100.41	99.6	99.82	100.38	99.63	100.32	100.15	99.6	99.56	100.05	100.59	99.43	99.65	100.06	99.69	100.3	99.79
Ba	35.6	96.3	18.6	31.6	23.9	17.8	34.1	23.9	23.8	113	110	11.7	22.1	21.5	20.3	18.7	22.5
Co	0.2	1.2	0.6	0.8	2	0.2	0.4	0.9	0.5	0.6	1.7	1.6	0.4	0.4	0.5	0.3	0.2
Cr	7.3	19.2	7.3	9.3	14	5.2	6.4	5.4	18.2	16.8	25.1	5.6	8.2	2.6	3.4	3.2	4.8
Cu	9	7.3	10.4	9.8	5.5	8	7.4	11.4	10.5	7.3	7.1	7.9	8.5	5.7	5.5	5.9	7.6
Ga	33.2	30	33.7	32.9	33	35.9	35.6	37.1	35	28.4	27.8	38.2	28.2	35.7	32.4	33.8	32.8
Nb	125	79	96	56	139	104	116	197	234	75	74	102	117	112	100	115	108
Ni	3.7	9.5	1.9	0.8	8.2	1.1	0.7	5.6	4.4	3.2	4.9	1.7	6.3	4.9	5.8	3.6	1.4
Pb	5.7	6.7	7.6	9.3	8.9	5.9	5.3	3.2	6.4	9.2	11.4	5.5	2.1	6.4	4.4	3.7	2.4
Rb	163	121	145	136	220	168	168	184	208	83	80	211	89	114	204	205	199
Sn	11	13.5	8.9	13.3	18.1	25.4	8.8	12.8	12.9	10.3	8.8	17	8.8	7.6	22.3	18.5	19.6
Sr	8.3	7.4	3.6	3	4.7	5	4.8	7.3	11.7	16.2	16.6	9.7	19.2	16.3	7	11.2	6.3
Ta	8.65	5.73	10.85	9.9	8.85	12.6	7.48	10.51	12.22	5.23	6.81	5.78	7.25	8.36	6.27	5.87	6.58
Th	14.1	13.9	12.3	18	15.7	20.1	18.4	20	23.5	9.4	8.2	11.3	16.5	14.1	12.5	17.7	13.9
U	7	5.8	5.8	7.2	8.5	5.7	5	13.3	14.7	4.8	4.3	5.3	5.5	6.8	4.3	7.7	6.1
V	2.4	1.7	0.4	1.7	0.8	1.1	0.4	0.3	2.5	3.2	3.8	1.2	1.9	1.6	2.1	0.9	1.2
Y	135	128	130	117	247	119	99	141	218	98	101	177	134	170	160	126	149
Zn	85	172	177	177	150	109	89	196	156	46	54	196	119	117	226	114	193
Zr	389	303	332	282	340	306	272	522	486	297	273	240	271	326	305	379	321
Hf	11.41	12.07	7.98	9.42	9.71	9.65	8.77	14.96	16.67	8.49	7.21	7.52	6.95	10.03	10.52	9.77	8.92
Cs	0.55	0.78	0.73	0.71	0.66	0.81	0.65	0.69	0.54	0.81	0.69	0.82	0.67	0.84	0.57	0.89	0.93
A/CNK	0.94	0.90	0.95	0.94	0.93	0.95	0.97	0.96	0.96	0.83	0.88	0.88	0.84	0.88	0.90	0.96	0.90
Rb/Sr	19.59	16.38	40.33	45.23	46.83	33.58	34.90	25.18	17.79	5.13	4.79	21.79	4.65	7.00	29.07	18.30	31.51
T_{Zrn}	847	810	829	807	824	823	818	878	865	796	793	774	801	808	812	841	818

Table 2. REEs contents of the granitic rocks of Mount El-Sibai in the Central Eastern Desert of Egypt.

Rock Type	Alkali-Feldspar Granites							Alkali-Amphibole-Bearing Granites			
Sample	SG1	SG10	SG11	SG14	SG30	SG31	SG39	SG46	SG47	SG49	SG50
La	11.39	22.54	22.67	25.81	15.72	16.35	22.67	24.62	25.81	33.74	33.19
Ce	20.85	46.00	47.32	62.46	31.40	32.78	47.32	66.14	66.40	84.61	85.35
Pr	2.56	5.24	5.37	7.85	3.37	3.50	5.37	9.33	8.68	11.31	10.71
Nd	9.69	19.19	20.41	30.47	15.31	14.35	20.41	34.75	35.56	44.62	43.58
Sm	3.38	4.41	5.81	8.77	4.49	3.81	5.81	9.36	9.31	13.04	12.62
Eu	0.09	0.40	0.64	1.01	0.16	0.17	0.34	0.27	0.31	0.80	0.75
Gd	4.76	8.02	9.70	9.54	6.74	6.91	7.70	7.32	10.09	14.37	13.86
Tb	1.26	2.49	2.65	1.68	1.87	1.93	1.95	1.91	1.79	2.73	2.78
Dy	11.20	20.28	20.62	11.66	15.67	15.93	15.62	14.14	15.78	18.60	18.19
Ho	2.71	5.35	5.80	2.50	3.68	3.94	3.30	2.96	3.73	3.66	3.58
Er	9.65	16.92	17.45	7.90	14.13	13.93	12.45	9.90	10.23	11.17	10.77
Tm	1.68	2.90	3.01	1.11	2.34	2.24	1.95	2.06	1.99	1.51	1.48
Yb	11.64	20.35	20.68	8.26	15.60	16.09	15.68	11.78	13.88	10.10	10.14
Lu	1.66	2.77	2.94	1.25	2.19	2.25	1.74	1.79	1.62	1.48	1.47
Eu/Eu*	0.07	0.21	0.26	0.34	0.09	0.1	0.16	0.1	0.1	0.18	0.17
La_N/Lu_N	0.71	0.85	0.80	2.14	0.75	0.75	1.35	1.43	1.65	2.37	2.35
$TE_{1,3}$	1.08	1.14	1.08	1.07	1.08	1.09	1.14	1.23	1.05	1.12	1.13
Total REE	93	177	185	180	133	134	162	196	205	252	248
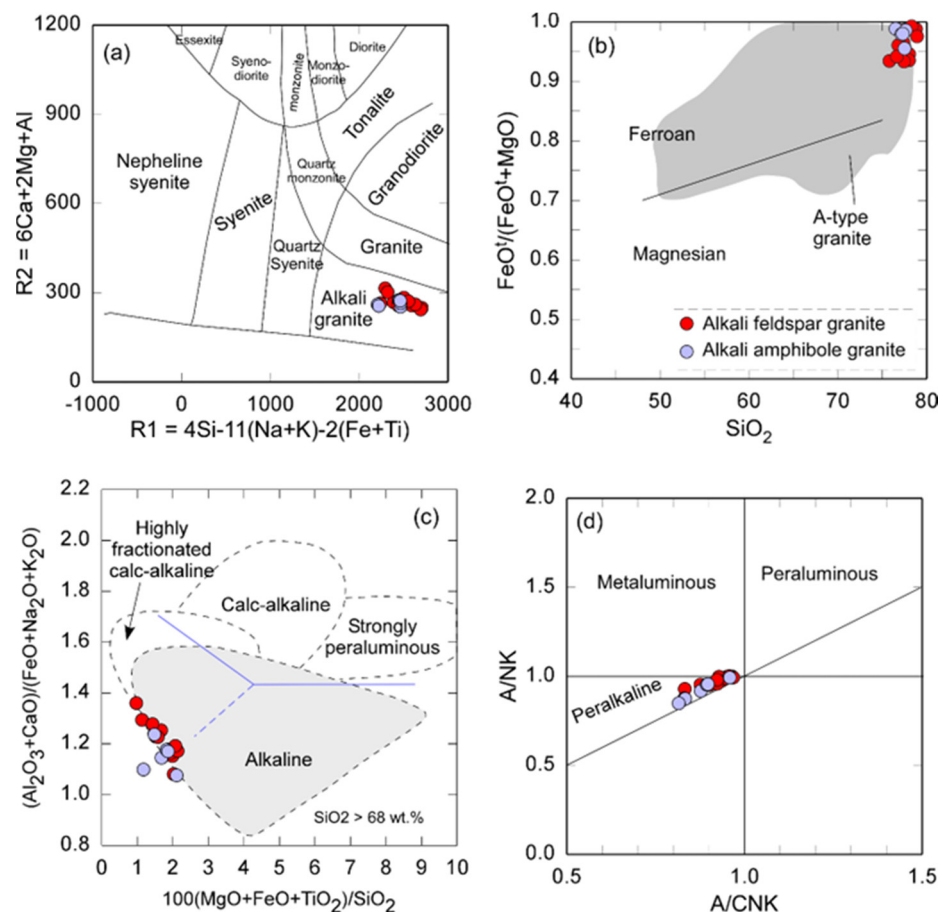
Figure 7. (**a**) R1–R2 diagram [36], which clearly indicate that Mount El-Sibai occupy the alkali granite field; (**b**) SiO_2 vs. $FeO^t/FeO^t + MgO$ binary diagram showing that Mount El-Sibai are ferroan and fall in the A-type granites field [34]; (**c**) major element classification diagram ($SiO_2 > 68\%$), after Sylvester [35] showing the fields of alkaline, calc-alkaline and highly fractionated calc-alkaline rocks, and (**d**) A/NK (molar $Al_2O_3/Na_2O + K_2O$) vs. A/CNK (molar $Al_2O_3/CaO + Na_2O + K_2O$) [37], showing that almost all samples are of peralkaline nature.

The primitive mantle-normalized multi-element diagram for the AFGs and AAGs is shown in Figure 8a. It is clear that both granitic types show general similarities in their patterns. They are enriched in some LILE (Rb, K, and Th) and HFSE (Ta, Pb, Zr, and Y), but strongly depleted in Ba, Sr, P and Ti, consistent with an A-type granite geochemical signature [38]. The chondrite-normalized REE patterns are presented in Figure 8b. The AAG exhibits slightly higher REE abundances (196–252 ppm; average 225 ppm) compared to the AFG (93–185 ppm; average 152 ppm). Additionally, the REE patterns of the AFG show less fractionation [$(La/Lu)_N$ = 0.71–2.14] in comparison to the AAG [$(La/Lu)_N$ = 1.43–2.37]. The Eu/Eu* values range from 0.07 to 0.34 in the AFG and reach extremely low values (0.10–0.18) in the AAG, indicating significant fractionation of the alkali feldspar [3].
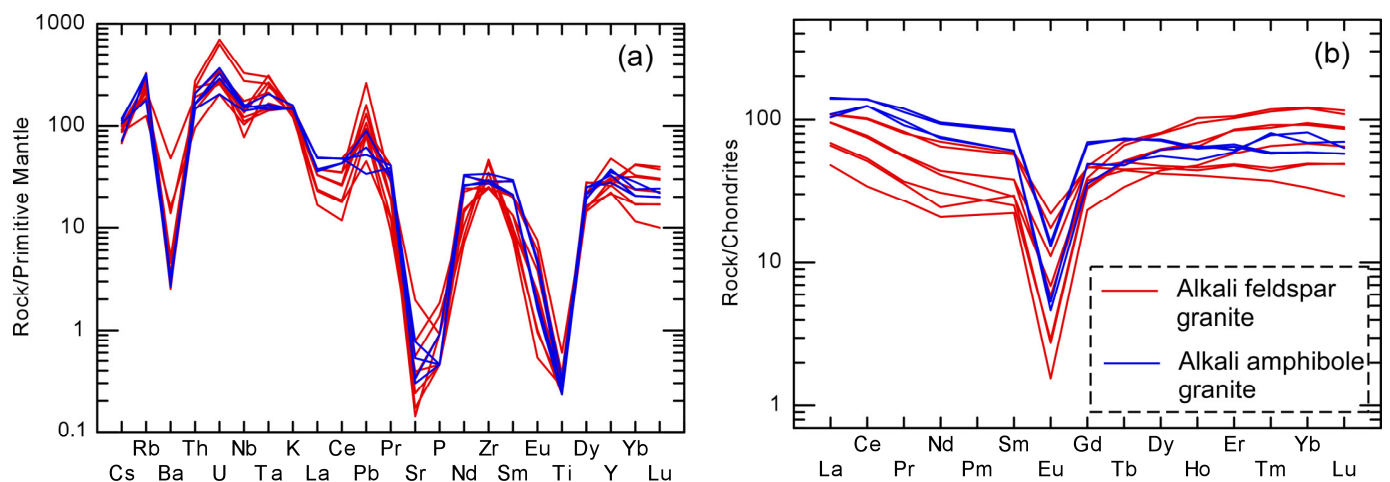
Figure 8. Primitive mantle-normalized trace element plots (**a**), and chondrite-normalized REE patterns (**b**) of Mount El-Sibai granites. The primitive mantle and normalization values are from Sun and McDonough [39].

5. Discussion

The preceding sections demonstrate that the Mount-El-Sibai granites consist of two primary types of rocks: AFG, which constitutes most of the pluton, and AAG, found in the outer regions. These rock varieties exhibit distinct compositions in terms of minerals and overall chemical makeup. Hence, it is crucial to establish the genetic relationship between these two facies. The presence of AAG, located at the periphery of the pluton and displaying transitional contacts with the AFG, suggests that they were formed either during the evolution of a substantial volume of magma or because of hydrothermal alteration of the AFG. This scenario is comparable to typical post-collisional granites found in the northern ANS, such as the zoned Katrina pluton in South Sinai [40] and the Abu-Diab granites in CED [9].

5.1. Magmatic vs. Metasomatic Origin of Silicate and Ore Minerals

The granitic rocks under investigation display an intriguing characteristic whereby they all consist of quartz, albite, K-feldspar, and biotite with similar chemical compositions. However, arfvedsonite is exclusively found in the AAG samples. The mineral texture and chemistry of Mount El-Sibai provide evidence that these rocks crystallized directly from a granitic magma and underwent late- to post-magmatic fluid fractionation processes, particularly in the AAG samples. The homogeneous composition and coexistence of albite, biotite, and K-feldspar as well-formed crystals indicate a magmatic origin (Figure 3). Additionally, the chemical composition of biotite and arfvedsonite supports their magmatic origin (Figure 4c–e). The occurrence of fluorite exclusively in the AAG samples suggests, on the other hand, the influence of late- to post-magmatic fluids during the evolution of AAG.

Metasomatism by late- to post-magmatic fluids is also evidenced by the alteration of a few albite and biotite crystals into sericite and chlorite, respectively. Furthermore, the presence of fine-grained albite surrounding quartz and K-feldspar in the AAG samples (Figure 3e) indicates the later formation of albite.

Based on textural characteristics, it is evident that the rare metal-bearing minerals are primarily associated with fluorite, which is one of the last phases to crystallize. Fluorite typically occurs as irregular grains between the rock-forming minerals (Figure 5b), indicating its magmatic origin. The presence of magmatic fluorite and the absence of titanite in the AAG samples suggest that moderate concentrations of fluorine (<1 wt.%) may be inherent characteristics of these magmas [41]. Experimental studies have shown the magmatic crystallization of Nb-Ta-bearing minerals in granitic rocks [42]. The presence of homogeneous anhedral to subhedral nioboaeschynite and columbite crystals as accessory phases within and/or between the rock-forming minerals further suggests their primary magmatic crystallization (Figure 5c–e).

Experimental data indicate that columbite can crystallize early from a magma melt with MnO + FeO contents >0.05 wt.% and Nb concentrations of approximately 70–100 ppm at relatively low temperatures (~600 °C) [42]. Moreover, magmatic systems can become enriched in F and Li at crystallization temperatures of around 650 °C [43]. Consequently, the AAG samples, with Nb concentrations of 100–117 ppm and relatively high MnO + Fe_2O_3 contents (0.94–1.74 wt.%), at slightly higher temperatures (T_{Zr} = 830 °C and T_{Ap} = 795 °C, on average; Table 1), indicate early saturation of magmatic columbite in the AAG magma.

Zircon is considered an excellent indicator of rare metals such as Nb, Ta, Y, and U [44]. In comparison to the AFG samples, zircon in the AAG samples spatially associates with thorite, fluorite, and columbite (Figure 5), suggesting its crystallization from a highly fractionated fluid-rich magma relative to the AFG magma. The Th/U ratios are also employed as an indicator of zircon type, where magmatic zircon has a ratio of 0.32–0.70, while hydrothermal zircon has a ratio of <0.1 [30]. Zircon from both types of granitic rocks exhibits Th/U ratios between 0.17 and 2.58 (Supplementary Table S5), confirming their magmatic origin.

5.2. Condition of Magma Crystallization

The granitic rocks from Mount El-Sibai exhibit a hypersolvus nature, indicating that they were formed at high temperatures and under low water pressure conditions. This characteristic is consistent with other alkaline rocks that are typically emplaced at relatively shallow depths [45].

In controlled laboratory conditions, alkali-amphibole (arfvedsonite) has been observed to crystallize from magma at pressures of approximately 150 MPa when the melt composition contains more than 4 wt.% H_2O [46]. Furthermore, the presence of magmatic fluids rich in fluorine aids in stabilizing alkali-amphiboles, particularly arfvedsonite, at lower pressures [47]. Temperature measurements of Mount El-Sibai magmas have been determined using the zircon-saturation thermometer model of Gervasoni et al. [48]. The zircon-saturation temperatures (T_{Zrn}) range from 793 to 878 °C for AFGs and from 774 to 841 °C for AAGs (Table 1). These elevated T_{Zrn} in the studied granites indicate that the magma from which the AFG and AAG crystallized was significantly hot, promoting the saturation of zircon. The calculated T_{Zrn} surpass the solidus temperature (700 °C) of granitic systems characterized by moderate H_2O content and low concentrations of F, B, and Li [49]. Consequently, the calculated temperatures should be considered as the minimum temperatures for the original magma.

5.3. Petrogenetic Type, Tectonic Setting, and Magma Type

It is difficult to distinguish A-type granites from highly fractionated I- and S-type granites with SiO_2 < 72 wt.% due to their similarity in both chemical and mineralogical composition [50,51]. However, several characteristics, such as the high 10,000 Ga/Al ratios (<4), and Na_2O + K_2O/CaO ratios (<10), and peralkaline natures, demonstrate that the

Mount El-Sibai granites show an affinity to A-type granites, rather than fractionated I-type and S-type granites [51,52]. This is further supported by the following: (1) the slightly higher alkali contents and large ion lithophile elements (LILE) abundances, including Rb, Cs, and K (Table 1), enrichment in some high field strength elements (HFSEs; e.g., Ga, Zn, Y, Ta and Nb) and strong depletion of Ba, Sr, Ti, and P (Figure 8a,b), which is consistent with the element compositional patterns of A-type granites [38]; (2) in the discrimination diagrams of $Na_2O + K_2O/CaO$, K_2O/MgO, Nb and Eu/Eu* vs. 10,000 Ga/Al (Figure 9a–d), they all plot in the A-type granite field [50]; and (3) the granitoids occupy the field of A-type granites in other geochemical diagrams (Figure 7b).
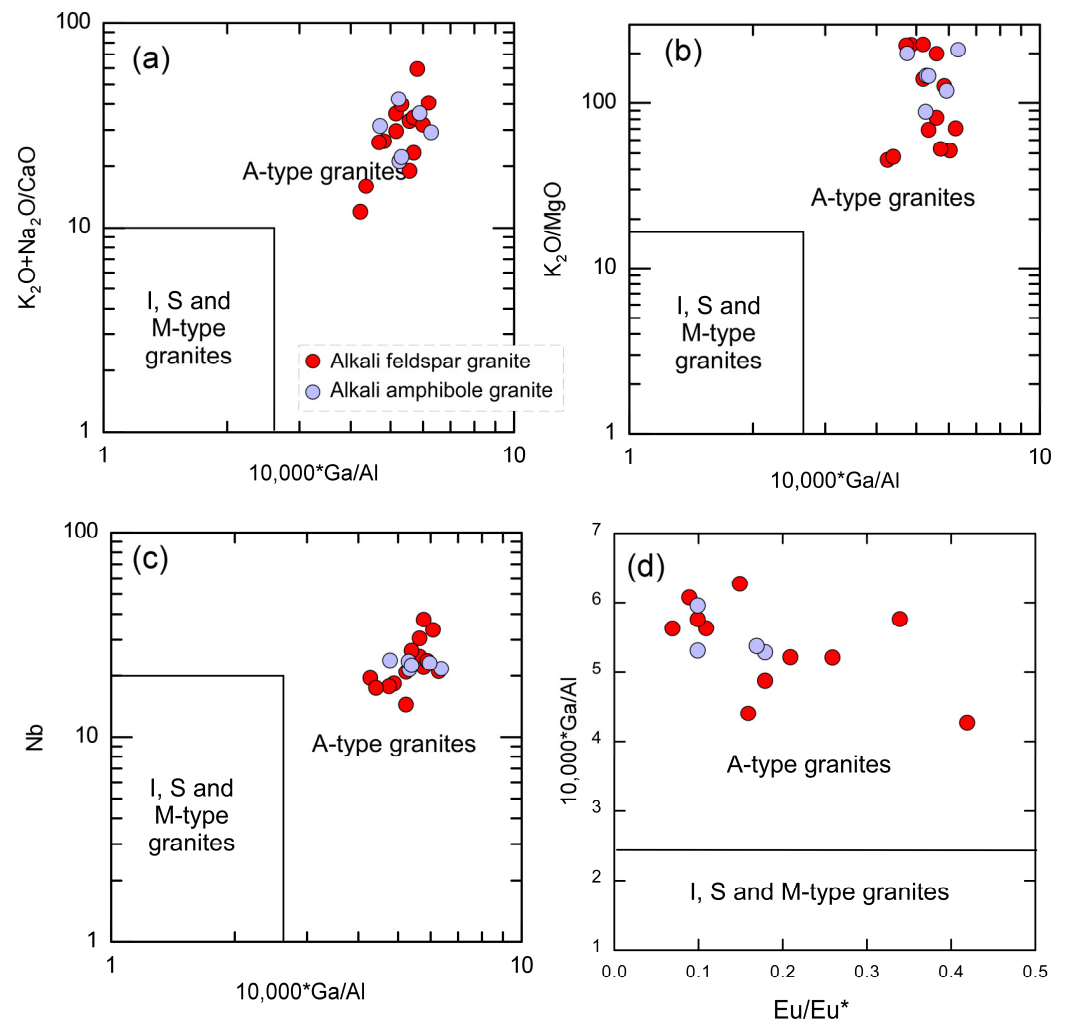
Figure 9. (**a–d**) Chemical classification diagrams (after Whalen et al., [50]), where granites samples plot in the A-type granites.

Based on the Zr/Hf ratio in zircon, A-type granites can be subdivided into three main categories: (1) normal granites with Zr/Hf > 55; (2) moderately fractionated granites with Zr/Hf varying between 55 and 25; and (3) strongly fractionated granites with Zr/Hf < 25 [53]. Accordingly, AFG (avg. Zr/Hf_{zircon} = 66) is classified as a normal granite, while AAG (Avg. Zr/Hf_{zircon} = 55) is a moderately fractionated granite (Supplementary Table S5).

On the tectonic discrimination diagram of Y vs. Nb and Yb = Ta vs. Rb by Pearce et al. [54], the geochemical affinity of the studied granites aligns with the within-plate field (Figure 10a,b). The plots on the primitive mantle normalized diagrams (Figure 8a) demonstrate enrichment in both large ion lithophile elements (LILE) and HFSE with an absence of negative Nb anomalies, indicating the formation of Mount El-Sibai in a within-

plate tectonic environment [54]. In synthesis, the geochemical data confirm that the Mount El-Sibai granites are within-plate anorogenic granites, which are commonly associated with crustal extension and/or rifting.
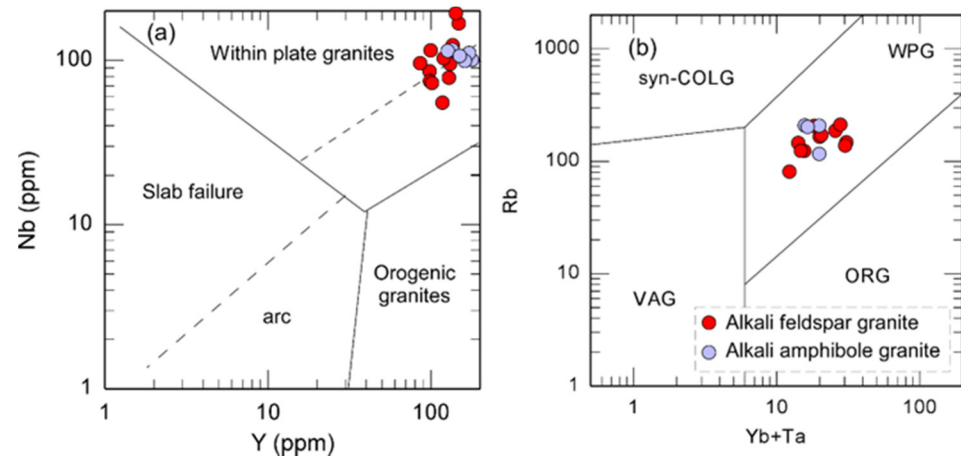
Figure 10. (**a**) Nb vs. Y and (**b**) Rb vs. Yb + Ta tectonic discrimination diagram of Pearce et al. [54], where the studied granitoids occupy the field of within-plate granites.

The composition of feldspars, amphiboles, and biotite in the studied granites also provide criteria for their tectono-magmatic affiliation, confirming and refining the inferences from whole-rock geochemistry. The alkali feldspars show no significant zoning, suggesting near-equilibrium crystallization conditions. They exhibit lower $CaO/(Na_2O + K_2O) \sim 0.006$ ratios compared to their host rocks (~0.06), indicating the alkaline–peralkaline nature of these rocks. Additionally, the AAG contains sodic amphiboles, indicating a peralkaline tendency. The composition of igneous biotite can be used to identify the nature of the host magmas. In the case of the analyzed biotite in both granitic types, they exhibit extremely high FeO content ranging from 33.33 to 34.97 wt.% with an average of 34.26 wt.% in AFGs and from 33.98 to 34.42 with an average of 34.27 in AAGs. These values closely resemble those found in biotite from alkaline, anorogenic granites (average 30.06 wt.%) (Figure 4b).

In general, peralkaline A-type granites require significantly higher temperatures during their formation compared to other granitoids, indicating the involvement of mantle-derived magmas in their genesis [45]. Despite the overall A-type affinity of Mount El-Sibai granites, assessing the relative contributions from mantle and crustal magmatic sources is challenging due to the juvenile nature of the Nubian Shield [5].

5.4. Petrogenesis of Mount El-Sibai Granites

Various petrogenetic models have been proposed to explain the formation of A-type rocks in general [55] and in the ANS in particular [56–58]. However, no single model adequately explains the wide range of chemical compositions observed among these granitic rocks. The substantial variations in isotope ratios and major and trace element concentrations strongly suggest that A-type granitic rocks originate from diverse processes and sources [59,60]. Some suggested models for the generation of A-type rocks in the ANS include fractional crystallization of mafic magma derived from the mantle [61], partial melting of different pre-existing crustal rocks [62], and a combination of mantle-derived sources with crustal materials [63]. The field relationships, chemical compositions, and petrological characteristics of Mount El-Sibai AFGs and AAGs provide evidence for their genetic association. Fieldwork observations indicate a sequence of intrusion in Mount El-Sibai granites, suggesting emplacement in two phases. However, the presence of both gradational and sharp contacts between the phases implies a short time interval between their emplacement before the complete crystallization of the first phase AFG (Figure 2a). The absence of compositional gaps in major and trace elements compositions (Tables 1

and 2), suggests that the Mount El-Sibai granites share a common parental magma that underwent magmatic fractionation processes.

The Mount El-Sibai granites exhibit characteristics of highly fractionated A-type granite, including elevated concentrations of Rb (80–220 ppm), Nb (56–234 ppm), Y (98–247 ppm), Zr (240–522 ppm), and Ta (5.2–12.6 ppm), but lower concentrations of Ba (12–113 ppm) and Sr (3–19 ppm) (Table 1). The geological and geochemical data suggest that these granites were emplaced in a post-collisional within-plate tectonic setting (Figure 10a,b). According to the Y-Nb-3Ga discrimination ternary diagram by Eby [52], the Mount El-Sibai granites almost fall within the A2 field (Figure 11a). This is further supported by the molar ($Na_2O + K_2O$)—vs. $Fe_2O_3^* \times 5$ vs. ($CaO + MgO$) × 5 ternary diagram by Grebennikov [64], where all the samples align with the A2-type field (Figure 11b). Therefore, the studied A-type granites are believed to have formed through partial melting of pre-existing crustal rocks with a contribution from the mantle. The mantle signature in the A-type granites of the ANS is likely due to the partial melting of juvenile continental crust [6].
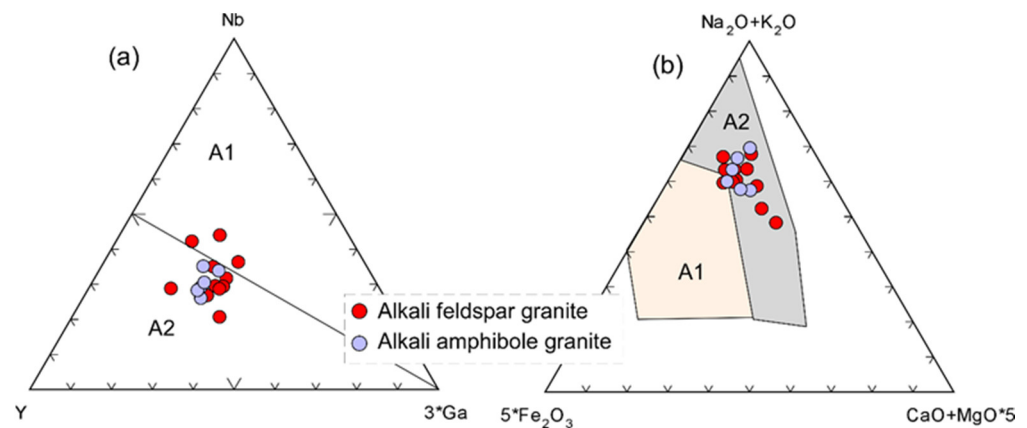
Figure 11. (**a**) Y-Nb-3Ga ternary plot [52]; A1 = A-type granitoids with an ocean island basalt–type source; A2 = A-type granitoids with crust-derived magma, and (**b**) $Na_2O + K_2O$ vs.—$Fe_2O_3^* \times 5$ vs. ($CaO + MgO$) × 5 (mol. quant.) [64]. A1 Field of silicic rocks of within-plate geodynamic settings: oceanic islands and continental rifts; A2, felsic igneous rock associations of intracontinental and continental-margin geodynamic settings.

The low concentrations of Co (0.20–2.0 ppm), Ni (0.7–9.5 ppm), and V (0.3–3.8 ppm) provide (Table 1), evidence against the hypothesis of extensive fractional crystallization of mantle-derived mafic magma. Furthermore, the abundance of felsic rocks in Mount El-Sibai cannot be explained solely by the fractional crystallization of mafic magma. Numerous geological, geochemical, and isotopic characteristics of the A-type rocks of the ANS contradict the idea of a mantle source [9,65].

Considering the fact that mantle materials typically exhibit very low Rb/Sr ratios ranging from 0.1 to 0.01 [66], while the lower and middle continental crusts have Rb/Sr ratios of 0.12 and 0.22, respectively [67], the elevated Rb/Sr ratios (4.6–46.8) observed in the studied granites argue against pure mantle origin and suggest a significant contribution of crustal materials to their formation. Plotting the samples on the Nb/Y versus Rb/Y diagram (Figure 12a) reveals that they align closely with values characteristic of the lower-to-upper crust, implying that melting and subsequent differentiation of crustal magmatic sources could account for the generation of the Mount El-Sibai granites. Therefore, it can be argued that these granites are predominantly derived from crustal magmatic sources with a minor contribution from the mantle, which likely provided the necessary heat for crustal melting.

The relatively high concentrations of K_2O in the granites are more likely a result of fractionation dominated by plagioclase and/or partial melting of crustal rocks, rather than

being derived from the mafic melts originating from the mantle. Furthermore, the samples show linear relationships in the (Ce/Zr)–Ce and (La/Hf)–La diagrams (Figure 12b,c), suggesting a petrogenetic process involving partial melting rather than fractional crystallization [68]. Therefore, Mount El-Sibai granites were most likely generated through partial melting of a juvenile crustal source followed by a magmatic fractionation process.
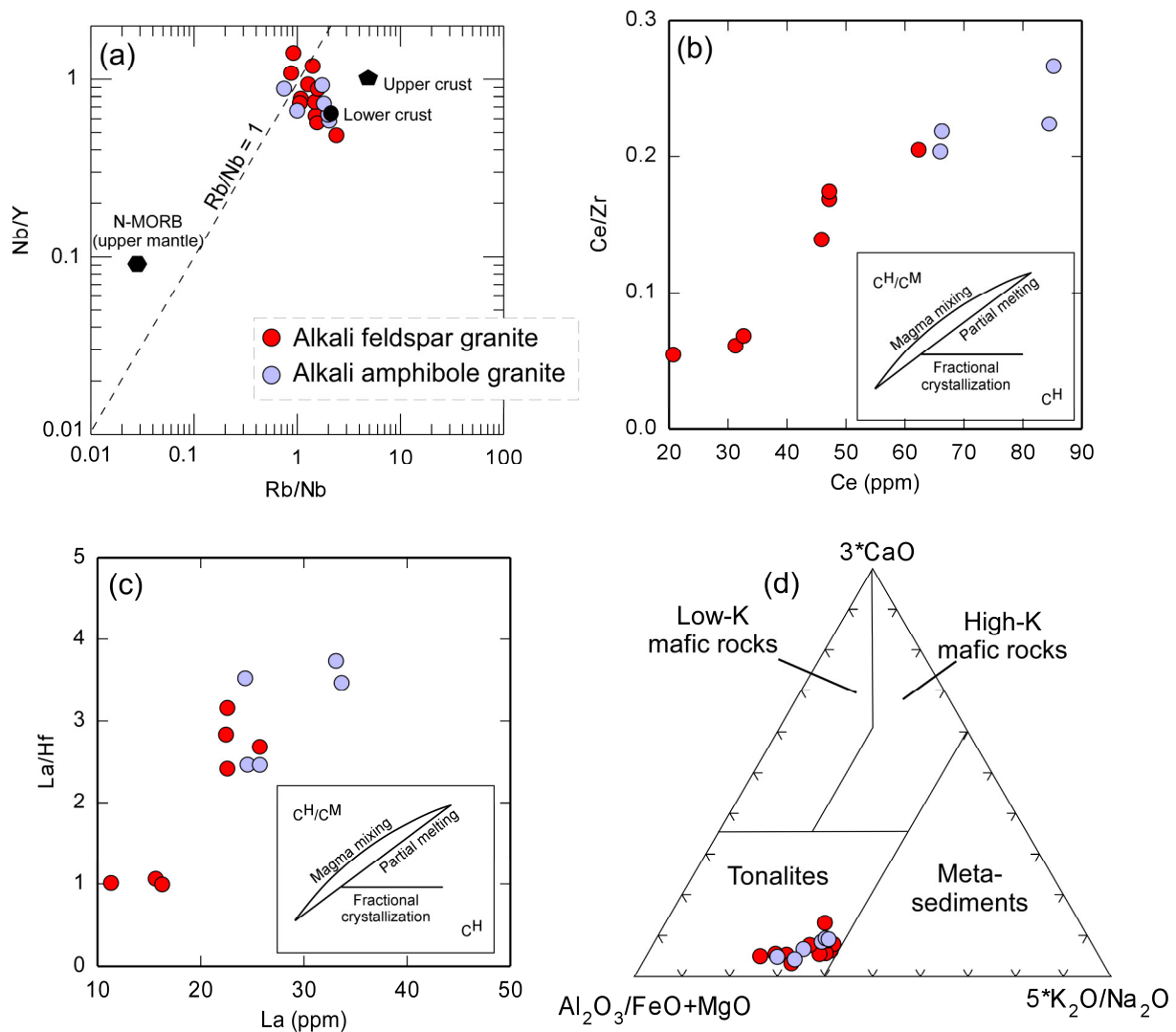
Figure 12. (**a**) Rb/Y versus Nb/Y diagram [69]. The composition of the upper and lower crust is adapted from Rudnick and Gao [70], while the N-MORB (normal mid-ocean ridge basalt) value is from Sun and McDonough [39], (**b**) Ce/Zr vs. Ce diagram [68], (**c**) La/Hf vs. La diagram [68] and (**d**) ternary diagram of $Al_2O_3/(FeO^t + MgO)$ vs. $3*CaO$ vs. $5*(K_2O/Na_2O)$ [71].

Possible crustal sources for the parental melt of the Mount El-Sibai granites include Neoproterozoic upper crustal rocks such as schists, gneisses, metagabbro-diorites, and I-type calc-alkaline granitoids. The presence of gneissic granites in the core of the El-Sibai intrusion further supports the idea of their origin through partial melting of a juvenile crustal source. Plotting the samples on a tonalites source diagram (Figure 12d) further confirms their derivation from the melting of an intermediate crustal magma source [71]. This is consistent with experimental studies indicating that dehydration melting of calc-alkaline tonalite at 950 °C and 0.4 GPa can produce melts with major and trace element characteristics resembling those of A-type magmas [72]. The intrusion of El-Sibai granites within the older tonalite–granodiorite association also provide a support for intermediate crustal magma source.

The available geochemical data and the consistent patterns of normalized trace elements and REEs (Figure 8a,b) support the hypothesis of magmatic differentiation from a shared parental magma. The primary fractionated phases include feldspars, with minor contributions from mafic minerals, apatite, and Fe-Ti oxides. The multielement spider diagram (Figure 8a) exhibit significant depletion in Eu, Ba, and Sr, which may indicate feldspars fractionation or may reflect retention of plagioclase in the source during the partial melting event. However, the fractionation of feldspars is evident from the Sr versus Rb/Sr plot (Figure 13a), where a decrease in CaO and Na_2O with increasing SiO_2 aligns with plagioclase fractionation. The role of feldspar fractionation is also indicated by co-variation in Ba vs. Rb (Figure 13b), where Ba decrease with increasing Rb, enhancing the fractionation of both plagioclase and K-feldspar during the evolution of granites. The highly fractionated REE patterns observed in the Mount El-Sibai granites (Figure 8b), particularly the prominent negative Eu anomalies (Eu/Eu* = 0.07–0.34), provide compelling evidence for fractionation of feldspars. Furthermore, the conspicuous negative anomalies of Eu, Ba, P, Zr, and Ti (Figure 8a) suggest minor fractionation of apatite, zircon, and Fe-Ti oxide.
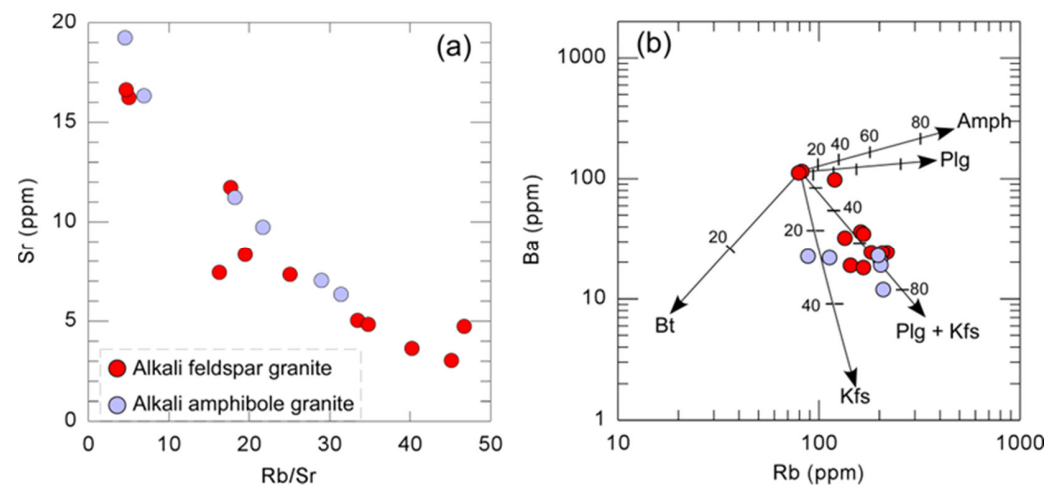
Figure 13. (**a**) Sr vs. Rb/Sr diagram, and (**b**) Ba vs. Rb diagram, showing that fractionation of K-feldspar and plagioclase. The Keskin [73] software was used to model the Rayleigh fractionation vectors.

The proposed model depicting the evolution of A-type rocks in the Mount El-Sibai region is illustrated in Figure 14. Initially, during the first stage, mantle-derived magma is generated as a consequence of lithospheric delamination caused by extension. This extension results in the upwelling of asthenospheric material, triggering extensive melting of certain sections of the lithospheric mantle. Additionally, the release of lithospheric extension pressure at depth leads to the influx of volatiles from deeper sources into the crust. The introduction of a volatile phase derived from the mantle brings additional heat, which lowers the melting temperature of rocks and initiates partial melting [74]. Shear zones and large-scale faults within the continental interior facilitate the ascent of the produced magma into the middle and upper crust, promoting the process of partial melting. Subsequently, the mingling and mixing of magmas give rise to magmatism with intermediate compositions that can evolve into felsic magmatism characterized by granitic compositions. The emplacement of the Mount El-Sibai granites most likely occurred following the termination of the Pan-African orogeny, along with the reactivation of Pan-African fractures. Quartz veins and shear zones cutting across the early phase of the Mount El-Sibai intrusion support an extensional tectonic regime during the emplacement of the studied A-type granites. The proposed geotectonic model for the generation of the Mount El-Sibai shares similarities with the lithospheric delamination model suggested by several authors to explain the evolution of the post-collisional alkaline/peralkaline phase in the ANS [75,76].
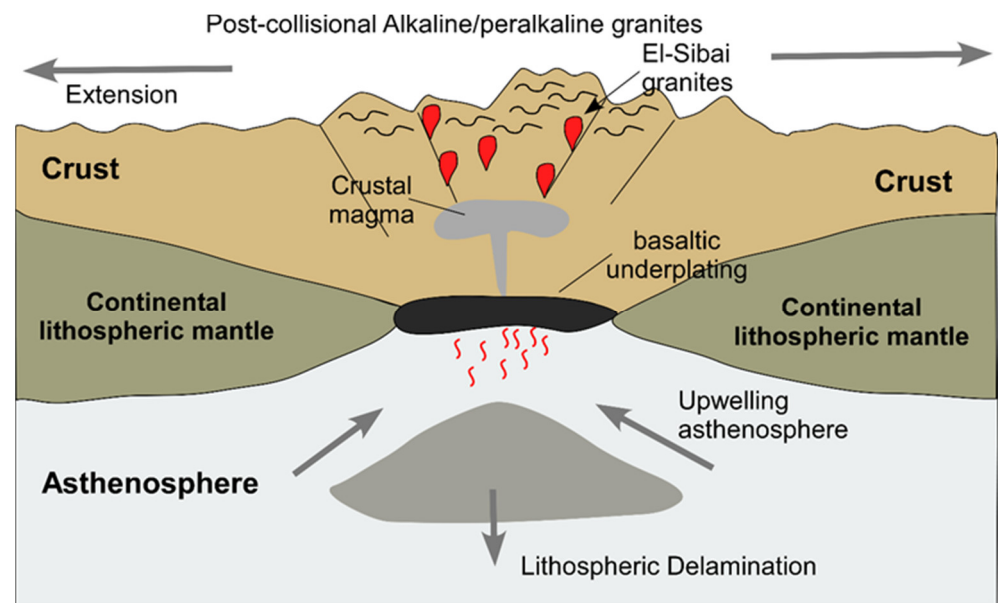
Figure 14. A simplified diagram illustrating the tectonomagmatic evolution of the A-type granites in Mount El-Sibai, highlighting the process of partial melting in the lower crust caused by the upwelling of mantle material from the asthenosphere due to lithospheric delamination. Not to scale.

5.5. The Role of Fluids on Rare-Metal Mineralization

It is worth noting that the fractionation of K-feldspar and/or mica alone cannot fully explain the various geochemical characteristics of Mount El-Sibai, such as the enrichment in most highly incompatible elements (Nb, Ta, U, Th, and Y) and the significant depletion in Sr and Ba. By applying the quantification method proposed by Irber [77], both granitic types exhibit a slightly elevated tetrad effect values ($TE_{1,3} > 1$; Table 2). The occurrence of the tetrad effect also appeared on the granite's REE pattern (Figure 8b). This suggests the influence of magmatic–fluid interaction processes in the formation of the Mount El-Sibai granites [78–80]. Previous studies by London et al. [81] have demonstrated that the incorporation of volatile elements like Li, F, and P in the magmatic system can have a significant impact on the solubility of Nb and Ta in the melt. In comparison to the AFG, the AAG meets the criteria of fluorine-rich granites found worldwide [82]. Therefore, the presence of magmatic fluorite in the AAG suggests that the high concentrations of Ta, Y, U, Th, and Nb are likely associated with the enrichment of volatile elements such as Li, F, and P during the magmatic evolution of the AAG. These volatile elements can form stable alkali–fluoro complexes that incorporate HFSEs within the AAG [82]. The elevated activity of F can also enhance magmatic differentiation by promoting a higher rate of fractional crystallization [5]. The occurrence of fluorite in the AAG samples clearly indicates the significant role of magmatic volatiles/fluids in the formation of these granites. The substantial presence of fluorine in the magma acts as a complexing agent, increasing the solubility of HFSEs, including Y, Nb, and Ta, leading to their incompatible behavior during magmatic differentiation. Consequently, the generated peralkaline granitic magma becomes enriched with ore metals such as Y, Nb, and Ta hosted by rare metal-bearing minerals (e.g., columbite, nioboaeschynite, zircon, and thorite) through prolonged fractionation processes.

6. Conclusions

The Mount El-Sibai granitic pluton is a prominent mountainous region in the central Eastern Desert of Egypt. The pluton primarily consists of alkali-feldspar granites (AFGs) with small amounts of alkali-amphibole-bearing granites (AAGs). The AFGs and AAGs are almost identical, with the primary distinguishing feature being the higher abundance of alkali-amphiboles in the AAG. The AAGs host special rare metal-bearing minerals (e.g.,

zircon, columbite, thorite, nioboaeschynite, and fluorite). Biotite in both rocks is classified as Fe-biotite with a typical alkaline magmatic signature. Amphiboles are classified as Na-amphibole with arfvedsonite composition. Columbite and nioboaeschynite are the main Nb-Ta bearing phase in AAGs. They occur as intergrown crystals or as independent crystals between the major mineral phases such as quartz and plagioclase. Columbite has a typical ferrocolumbite composition.

Both granites exhibit a highly evolved and peralkaline nature. They are enriched in some LILE (Rb, K, and Th) and HFSE (Ta, Pb, Zr, and Y), but strongly depleted in Ba, Sr, P and Ti, with prominent negative Eu anomaly, consistent with an A-type granite geochemical signature. The texture and chemistry of minerals provide evidence that these rocks crystallized directly from a granitic magma and later underwent late- to post-magmatic fluid fractionation processes, particularly in the AAG samples. The elevated T_{Zrn} values indicate that the magma from which the granites were formed, was significantly hot. Geochemically, the granites are enriched in both LILEs and HFSEs with an absence of negative Nb anomalies, confirming their formation in a within-plate anorogenic tectonic setting associated with crustal extension and/or rifting.

We argue that the studied granites have been formed through partial melting of pre-existing intermediate crustal rocks. The geochemical data support the formation of Mount El-Sibai by magmatic differentiation from a common parental magma. The primary fractionated phases include feldspars, with minor contributions from mafic minerals, apatite, and Fe-Ti oxides. The lithospheric delamination process caused the upwelling of asthenospheric material and triggered extensive melting of the overlaying lithospheric mantle material. This leads to the influx of volatiles from deeper sources into the crust. These volatiles, especially fluorine-formed complexes of rare metal elements (e.g., Nb, Ta, Sn and REEs), preserved the melt structure and thus were not included in the early fractional crystallization. Consequently, the generated peralkaline granitic magma becomes enriched with ore metals such as Y, Nb, and Ta hosted by rare metal-bearing minerals (e.g., columbite, nioboaeschynite, zircon, and thorite) through extensive and prolonged fractionation processes.

Author Contributions: Conceptualization, M.S., A.F.A., K.S.Z. and H.O.; methodology, R.A. and W.X.; software, I.V.S., K.A., M.S.F. and W.X.; validation, M.S., H.O. and H.A.; formal analysis, M.S., I.V.S. and R.A.; investigation, M.S.; resources, H.O.; data curation, M.S., H.A. and W.X.; writing—original draft preparation, M.S.; writing—review and editing, I.V.S. and W.X.; visualization, H.O.; K.A. and M.S.F.; supervision, M.S., A.F.A. and K.S.Z.; project administration, M.S.; funding acquisition, K.A., M.S.F. and I.V.S. All authors have read and agreed to the published version of the manuscript.

Data Availability Statement: Not applicable.

Conflicts of Interest: The authors declare no conflict of interest.

References

1. Siegel, K.; Vasyukova, O.V.; Williams-Jones, A.E. Magmatic evolution and controls on rare metal-enrichment of the Strange Lake A-type peralkaline granitic pluton, Québec-Labrador. *Lithos* **2018**, *308*, 34–52. [CrossRef]
2. Girei, M.B.; Li, H.; Algeo, T.J.; Bonin, B.; Ogunleye, P.O.; Bute, S.I.; Ahmed, H.A. Petrogenesis of A-type granites associated with Sn–Nb–Zn mineralization in Ririwai complex, north-Central Nigeria: Constraints from whole-rock SmNd and zircon LuHf isotope systematics. *Lithos* **2019**, *340–341*, 49–70. [CrossRef]
3. Abdel-Karim, A.-A.; Azer, M.; Sami, M. Petrogenesis and tectonic implications of the Maladob ring complex in the South Eastern Desert, Egypt: New insights from mineral chemistry and whole-rock geochemistry. *Int. J. Earth Sci.* **2020**, *110*, 53–80. [CrossRef]
4. Su, H.-M.; Jiang, S.-Y.; Zhu, X.-Y.; Duan, Z.-P.; Huang, X.-K.; Zou, T. Magmatic-hydrothermal processes and controls on rare-metal enrichment of the Baerzhe peralkaline granitic pluton, inner Mongolia, northeastern China. *Ore Geol. Rev.* **2021**, *131*, 103984. [CrossRef]
5. Sami, M.; El Monsef, M.A.; Abart, R.; Toksoy-Köksal, F.; Abdelfadil, K.M. Unraveling the Genesis of Highly Fractionated Rare-Metal Granites in the Nubian Shield via the Rare-Earth Elements Tetrad Effect, Sr–Nd Isotope Systematics, and Mineral Chemistry. *ACS Earth Space Chem.* **2022**, *6*, 2368–2384. [CrossRef]
6. Sami, M.; Adam, M.M.; Lv, X.; Lasheen, E.S.R.; Ene, A.; Zakaly, H.M.; Alarifi, S.S.; Mahdy, N.M.; Abdel Rahman, A.R.A.; Saeed, A. Petrogenesis and Tectonic Implications of the Cryogenian I-Type Granodiorites from Gabgaba Terrane (NE Sudan). *Minerals* **2023**, *13*, 331. [CrossRef]
7. Gamaleldien, H.; Li, Z.-X.; Anbar, M.A.; Murphy, J.B.; Evans, N.J.; Xia, X.-P. Formation of juvenile continental crust in northern Nubian Shield: New evidence from granitic zircon U-Pb-Hf-O isotopes. *Precambrian Res.* **2022**, *379*, 106791. [CrossRef]
8. Adam, M.M.A.; Lv, X.; Fathy, D.; Abdel Rahman, A.R.A.; Ali, A.A.; Mohammed, A.S.; Farahat, E.S.; Sami, M. Petrogenesis and tectonic implications of Tonian island arc volcanic rocks from the Gabgaba Terrane in the Arabian-Nubian Shield (NE Sudan). *J. Asian Earth Sci.* **2022**, *223*, 105006. [CrossRef]
9. Sami, M.; Ntaflos, T.; Farahat, E.S.; Mohamed, H.A.; Hauzenberger, C.; Ahmed, A.F. Petrogenesis and geodynamic implications of Ediacaran highly fractionated A-type granitoids in the north Arabian-Nubian Shield (Egypt): Constraints from whole-rock geochemistry and Sr-Nd isotopes. *Lithos* **2018**, *304–307*, 329–346. [CrossRef]
10. Mahdy, N.M.; Ntaflos, T.; Pease, V.; Sami, M.; Slobodník, M.; Abu Steet, A.A.; Abdelfadil, K.M.; Fathy, D. Combined zircon U-Pb dating and chemical Th–U–total Pb chronology of monazite and thorite, Abu Diab A-type granite, Central Eastern Desert of Egypt: Constraints on the timing and magmatic-hydrothermal evolution of rare metal granitic magmatism in the Arabian Nubian Shield. *Geochemistry* **2020**, *80*, 125669. [CrossRef]
11. Abd El Monsef, M.; Sami, M.; Toksoy-Köksal, F.; Abart, R.; Ondrejka, M.; Abdelfadil, K.M. Role of Magmatism and Related-Exsolved Fluids during Ta-Nb-Sn Concentration in the Central Eastern Desert of Egypt: Evidences from Mineral Chemistry and Fluid Inclusions. *J. Earth Sci.* **2023**. [CrossRef]
12. Khalil, A.E.S.; Obeid, M.A.; Azer, M.K.; Asimow, P.D. Geochemistry and petrogenesis of post-collisional alkaline and peralkaline granites of the Arabian-Nubian Shield: A case study from the southern tip of Sinai Peninsula, Egypt. *Int. Geol. Rev.* **2017**, *60*, 998–1018. [CrossRef]
13. Lundmark, A.M.; Andresen, A.; Hassan, M.A.; Augland, L.E.; Boghdady, G.Y. Repeated magmatic pulses in the East African Orogen in the Eastern Desert, Egypt: An old idea supported by new evidence. *Gondwana Res.* **2012**, *22*, 227–237. [CrossRef]
14. El-Sayed, M.M.; Mohamed, F.H.; Furnes, H.; Kanisawa, S. Geochemistry and petrogenesis of the Neoproterozoic granitoids in the Central Eastern Desert, Egypt. *Chem. Erde-Geochem.* **2002**, *62*, 317–346. [CrossRef]
15. Fritz, H.; Dallmeyer, D.R.; Wallbrecher, E.; Loizenbauer, J.; Hoinkes, G.; Neumayr, P.; Khudeir, A.A. Neoproterozoic tectonothermal evolution of the Central Eastern Desert, Egypt: A slow velocity tectonic process of core complex exhumation. *J. Afr. Earth Sci.* **2002**, *34*, 137–155. [CrossRef]
16. Peng, P.; Anbar, M.M.A.; He, X.-F.; Liu, X.; Qin, Z. Cryogenian accretion of the Northern Arabian-Nubian shield: Integrated evidence from central Eastern Desert Egypt. *Precambrian Res.* **2022**, *371*, 106599. [CrossRef]
17. Ali, S.; Abart, R.; Sayyed, M.I.; Hauzenberger, C.A.; Sami, M. Petrogenesis of the Wadi El-Faliq Gabbroic Intrusion in the Central Eastern Desert of Egypt: Implications for Neoproterozoic Post-Collisional Magmatism Associated with the Najd Fault System. *Minerals* **2023**, *13*, 10. [CrossRef]
18. Abdelfadil, K.M.; Saleh, G.M.; Putiš, M.; Sami, M. Mantle source characteristics of the late Neoproterozoic post-collisional gabbroic intrusion of Wadi Abu Hadieda, north Arabian-Nubian Shield, Egypt. *J. Afr. Earth Sci.* **2022**, *194*, 104607. [CrossRef]
19. Ali, S.; Ntaflos, T.; Sami, M. Geochemistry of Khor Um-Safi ophiolitic serpentinites, central Eastern desert, Egypt: Implications for neoproterozoic arc-basin system in the Arabian-Nubian shield. *Geochemistry* **2021**, *81*, 125690. [CrossRef]
20. Faisal, M.; Yang, X.; Zhang, H.; Amuda, A.K.; Sun, C.; Mustafa, S.; Gul, M.A. Mineralization Styles, Alteration Mineralogy, and Sulfur Isotope Geochemistry of Volcanogenic Massive Sulfide Deposits in the Shadli Metavolcanics Belt, South Eastern Desert, Egypt: Metallogenic Implications. *Ore Geol. Rev.* **2021**, *140*, 104402. [CrossRef]
21. Abdel-Rahman, A.M. Petrogenesis of anorogenic peralkaline granitic complexes from eastern Egypt. *Miner. Mag.* **2006**, *70*, 27–50. [CrossRef]
22. Frisch, W.; Abdel-Rahman, A.M. Petrogenesis of the Wadi Dib alkaline ring complex, Eastern Desert of Egypt. *Mineral. Petrol.* **1999**, *65*, 249–275. [CrossRef]

23. Abuamarah, B.A.; Azer, M.K.; Asimow, P.D.; Ghrefat, H.; Mubarak, H.S. Geochemistry and Petrogenesis of Late Ediacaran Rare-metal Albite Granites of the Arabian-Nubian Shield. *Acta Geol. Sin. Engl. Ed.* **2021**, *95*, 459–480. [CrossRef]

24. Gamal El Dien, H.; Li, Z.-X.; Abu Anbar, M.; Doucet, L.S.; Murphy, J.B.; Evans, N.J.; Xia, X.-P.; Li, J. The largest plagiogranite on Earth formed by re-melting of juvenile proto-continental crust. *Commun. Earth Environ.* **2021**, *2*, 138. [CrossRef]

25. Sami, M. Rare Metal Granites, Central Eastern Desert, Egypt: Geochemistry and Economic Potentiality. Ph.D. Thesis, Universiy of Vienna, Vienna, Austria, 2018.

26. Abdel-Rahman, A.F.M. Nature of Biotites from Alkaline, Calc-alkaline, and Peraluminous Magmas. *J. Petrol.* **1994**, *35*, 525–541. [CrossRef]

27. Nachit, H.; Ibhi, A.; Abia, E.H.; Ben Ohoud, M. Discrimination between primary magmatic biotites, reequilibrated biotites and neoformed biotites. *Comptes Rendus Geosci.* **2005**, *337*, 1415–1420. [CrossRef]

28. Leake, B.E.; Woolley, A.R.; Arps, C.E.; Birch, W.D.; Gilbert, M.C.; Grice, J.D.; Hawthorne, F.C.; Kato, A.; Kisch, H.J.; Krivovichev, V.G. Report. Nomenclature of Amphiboles: Report of the Subcommittee on Amphiboles of the International Mineralogical Association Commission on New Minerals and Mineral Names. *Miner. Mag.* **1997**, *61*, 295–321. [CrossRef]

29. Pe-Piper, G. Relationship of amphibole composition to host-rock geochemistry: The A-type gabbro-granite Wentworth pluton, Cobequid shear zone, eastern Canada. *Eur. J. Mineral.* **2007**, *19*, 29–38. [CrossRef]

30. Hoskin, P.W.O.; Schaltegger, U. The composition of zircon and igneous and metamorphic petrogenesis. *Rev. Miner. Geochem.* **2003**, *53*, 27–62. [CrossRef]

31. Deliens, M. Titanian Aeschynite-(Y) from Trimouns (French Pyrenees). *Bull. L'Institut R. Sci. Nat. Belg. Sci. Terre* **1991**, *61*, 231–236.

32. Sami, M.; Ntaflos, T.; Farahat, E.S.; Mohamed, H.A.; Ahmed, A.F.; Hauzenberger, C. Mineralogical, geochemical and Sr-Nd isotopes characteristics of fluorite-bearing granites in the Northern Arabian-Nubian Shield, Egypt: Constraints on petrogenesis and evolution of their associated rare metal mineralization. *Ore Geol. Rev.* **2017**, *88*, 1–22. [CrossRef]

33. Sami, M.; Mahdy, N.M.; Ntaflos, T.; Fathy, D. Composition and origin of Ti–Nb–Ta–Zr bearing minerals in the Abu Diab highly evolved granite from the Central Eastern Desert of Egypt. *J. Afr. Earth Sci.* **2020**, *165*, 103808. [CrossRef]

34. Frost, B.R.; Barnes, C.G.; Collins, W.J.; Arculus, R.J.; Ellis, D.J.; Frost, C.D. A geochemical classification for granitic rocks. *J. Petrol.* **2001**, *42*, 2033–2048. [CrossRef]

35. Sylvester, P.J. Post-collisional strongly peraluminous granites. *Lithos* **1998**, *45*, 29–44. [CrossRef]

36. De la Roche, H.; Leterrier, J.; Grandclaude, P.; Marchal, M. A classification of volcanic and plutonic rocks using R 1 R 2 -diagram and major-element analyses—Its relationships with current nomenclature. *Chem. Geol.* **1980**, *29*, 183–210. [CrossRef]

37. Maniar, P.D.; Piccoli, P.M. Tectonic discrimination of granitoids. *Geol. Soc. Am. Bull.* **1989**, *101*, 635–643. [CrossRef]

38. Wu, F.-Y.; Sun, D.-Y.; Li, H.; Jahn, B.-M.; Wilde, S. A-type granites in northeastern China: Age and geochemical constraints on their petrogenesis. *Chem. Geol.* **2002**, *187*, 143–173. [CrossRef]

39. Sun, S.-S.; McDonough, W.F. Chemical and isotopic systematics of oceanic basalts: Implications for mantle composition and processes. *Geol. Soc. Lond. Spec. Publ.* **1989**, *42*, 313–345. [CrossRef]

40. Katzir, Y.; Eyal, M.; Litvinovsky, B.A.; Jahn, B.M.; Zanvilevich, A.N.; Valley, J.W.; Beeri, Y.; Pelly, I.; Shimshilashvili, E. Petrogenesis of A-type granites and origin of vertical zoning in the Katharina pluton, Gebel Mussa (Mt. Moses) area, Sinai, Egypt. *Lithos* **2007**, *95*, 208–228. [CrossRef]

41. Price, J.D.; Hogan, J.P.; Gilbert, M.C.; London, D.; Morgan, G.B. Experimental study of titanite-fluorite equilibria in the A-type Mount Scott Granite: Implications for assessing F contents of felsic magma. *Geology* **1999**, *27*, 951–954. [CrossRef]

42. Linnen, R.L.; Keppler, H. Columbite solubility in granitic melts: Consequences for the enrichment and fractionation of Nb and Ta in the Earth's crust. *Contrib. Mineral. Petrol.* **1997**, *128*, 213–227. [CrossRef]

43. Dolejš, D.; Baker, D.R. Liquidus Equilibria in the System K2O–Na2O–Al2O3–SiO2–F2O−1–H2O to 100 MPa: II. Differentiation Paths of Fluorosilicic Magmas in Hydrous Systems. *J. Petrol.* **2007**, *48*, 807–828. [CrossRef]

44. Xiao, W.; Liu, C.; Tan, K.; Duan, X.; Shi, K.; Sui, Q.; Feng, P.; Sami, M.; Ahmed, M.S.; Zi, F. Two Distinct Fractional Crystallization Mechanisms of A-Type Granites in the Nanling Range, South China: A Case Study of the Jiuyishan Complex Massif and Xianghualing Intrusive Stocks. *Minerals* **2023**, *13*, 605. [CrossRef]

45. King, P.L.; White, A.J.R.; Chappell, B.W.; Allen, C.M. Characterization and origin of aluminous A-type granites from the Lachlan Fold Belt, Southeastern Australia. *J. Petrol.* **1997**, *38*, 371–391. [CrossRef]

46. Scaillet, B.; Macdonald, R. Phase Relations of Peralkaline Silicic Magmas and Petrogenetic Implications. *J. Petrol.* **2001**, *42*, 825–845. [CrossRef]

47. Scaillet, B.; Holtz, F.; Pichavant, M. Experimental Constraints on the Formation of Silicic Magmas. *Elements* **2016**, *12*, 109–114. [CrossRef]

48. Gervasoni, F.; Klemme, S.; Rocha-Júnior, E.R.V.; Berndt, J. Zircon saturation in silicate melts: A new and improved model for aluminous and alkaline melts. *Contrib. Mineral. Petrol.* **2016**, *171*, 21. [CrossRef]

49. Dall'Agnol, R.; Ramo, O.T.; de Magalhaes, M.S.; Macambira, M.J.B. Petrology of the anorogenic, oxidised Jamon and Musa granites, Amazonian Craton: Implications for the genesis of Proterozoic A-type granites. *Lithos* **1999**, *46*, 431–462. [CrossRef]

50. Whalen, J.B.; Currie, K.L.; Chappell, B.W. A-type granites: Geochemical characteristics, discrimination and petrogenesis. *Contrib. Mineral. Petrol.* **1987**, *95*, 407–419. [CrossRef]

51. Bonin, B. A-type granites and related rocks: Evolution of a concept, problems and prospects. *Lithos* **2007**, *97*, 1–29. [CrossRef]

52. Eby, G.N. The A-type granitoids: A review of their occurrence and chemical characteristics and speculations on their petrogenesis. *Lithos* **1990**, *26*, 115–134. [CrossRef]

53. Breiter, K.; Lamarao, C.N.; Borges, R.M.K.; Dall'Agnol, R. Chemical characteristics of zircon from A-type granites and comparison to zircon of S-type granites. *Lithos* **2014**, *192*, 208–225. [CrossRef]

54. Pearce, J.A.; Harris, N.B.W.; Tindle, A.G. Trace Element Discrimination Diagrams for the Tectonic Interpretation of Granitic Rocks. *J. Petrol.* **1984**, *25*, 956–983. [CrossRef]

55. Johansson, Å. A Tentative Model for the Origin of A-Type Granitoids. *Minerals* **2023**, *13*, 236. [CrossRef]

56. Abuamarah, B.A.; Azer, M.K.; Seddik, A.M.A.; Asimow, P.D.; Guzman, P.; Fultz, B.T.; Wilner, M.J.; Dalleska, N.; Darwish, M.H. Magmatic and post-magmatic evolution of post-collisional rare-metal bearing granite: The Neoproterozoic Homrit Akarem Granitic Intrusion, south Eastern Desert of Egypt, Arabian-Nubian Shield. *Geochemistry* **2022**, *82*, 125840. [CrossRef]

57. Gahlan, H.A.; Asimow, P.D.; Azer, M.K.; Ma, C.; Al-Kahtany, K.M.; Hakeem, A.Y. Geochemistry and mineralogy of the Jebel Aja Igneous Intrusion and the associated exotic pegmatites, Arabian Shield, Saudi Arabia. *Lithos* **2021**, 106395. [CrossRef]

58. Sami, M.; Ntaflos, T.; Mohamed, H.A.; Farahat, E.S.; Hauzenberger, C.; Mahdy, N.M.; Abdelfadil, K.M.; Fathy, D. Origin and Petrogenetic Implications of Spessartine Garnet in Highly-Fractionated Granite from the Central Eastern Desert of Egypt. *Acta Geol. Sin. Engl. Ed.* **2020**, *94*, 763–776. [CrossRef]

59. Ali, K.A.; Moghazi, A.-K.M.; Maurice, A.E.; Omar, S.A.; Wang, Q.; Wilde, S.A.; Moussa, E.M.; Manton, W.I.; Stern, R.J. Composition, age, and origin of the ~620 Ma Humr Akarim and Humrat Mukbid A-type granites: No evidence for pre-Neoproterozoic basement in the Eastern Desert, Egypt. *Int. J. Earth Sci.* **2012**, *101*, 1705–1722. [CrossRef]

60. Eliwa, H.A.; Breitkreuz, C.; Murata, M.; Khalaf, I.M.; Bulhler, B.; Itaya, T.; Takahashi, T.; Hirahara, Y.; Miyazaki, T.; Kimura, J.I.; et al. SIMS zircon U-Pb and mica K-Ar geochronology, and Sr-Nd isotope geochemistry of Neoproterozoic granitoids and their bearing on the evolution of the north Eastern Desert, Egypt. *Gondwana Res.* **2014**, *25*, 1570–1598. [CrossRef]

61. Jarrar, G.H.; Manton, W.I.; Stern, R.J.; Zachmann, D. Late Neoproterozoic A-type granites in the northernmost Arabian-Nubian Shield formed by fractionation of basaltic melts. *Chem. Der Erde Geochem.* **2008**, *68*, 295–312. [CrossRef]

62. Farahat, E.S.; Zaki, R.; Hauzenberger, C.; Sami, M. Neoproterozoic calc-alkaline peraluminous granitoids of the Deleihimmi pluton, Central Eastern Desert, Egypt: Implications for transition from late- to post-collisional tectonomagmatic evolution in the northern Arabian-Nubian Shield. *Geol. J.* **2011**, *46*, 544–560. [CrossRef]

63. Ali, K.A.; Kroner, A.; Hegner, E.; Wong, J.; Li, S.Q.; Gahlan, H.A.; Abu El Ela, F.F. U-Pb zircon geochronology and Hf-Nd isotopic systematics of Wadi Beitan granitoid gneisses, South Eastern Desert, Egypt. *Gondwana Res.* **2015**, *27*, 811–824. [CrossRef]

64. Grebennikov, A. A-type granites and related rocks: Petrogenesis and classification. *Russ. Geol. Geophys.* **2014**, *55*, 1353–1366. [CrossRef]

65. Moghazi, A.-K.M.; Iaccheri, L.M.; Bakhsh, R.A.; Kotov, A.B.; Ali, K.A. Sources of rare-metal-bearing A-type granites from Jabel Sayed complex, Northern Arabian Shield, Saudi Arabia. *J. Asian Earth Sci.* **2015**, *107*, 244–258. [CrossRef]

66. Hofmann, A.W. Chemical differentiation of the Earth: The relationship between mantle, continental crust, and oceanic crust. *Earth Planet. Sci. Lett.* **1988**, *90*, 297–314. [CrossRef]

67. Wedepohl, K.H. The Composition of the Continental-Crust. *Geochim. Et Cosmochim. Acta* **1995**, *59*, 1217–1232. [CrossRef]

68. Schiano, P.; Monzier, M.; Eissen, J.P.; Martin, H.; Koga, K.T. Simple mixing as the major control of the evolution of volcanic suites in the Ecuadorian Andes. *Contrib. Mineral. Petrol.* **2010**, *160*, 297–312. [CrossRef]

69. Chazot, G.; Bertrand, H. Genesis of silicic magmas during tertiary continental rifting in Yemen. *Lithos* **1995**, *36*, 69–83. [CrossRef]

70. Rudnick, R.L.; Gao, S. 3.01—Composition of the Continental Crust A2—Holland, Heinrich D. In *Treatise on Geochemistry*; Turekian, K.K., Ed.; Pergamon: Oxford, UK, 2003; pp. 1–64.

71. Laurent, A.; Janousek, V.; Magna, T.; Schulmann, K.; Mikova, J. Petrogenesis and geochronology of a post-orogenic calc-alkaline magmatic association: The Zulova Pluton, Bohemian Massif. *J. Geosci.* **2014**, *59*, 415–440. [CrossRef]

72. Patiño Douce, A.E. Generation of metaluminous A-type granites by low-pressure melting of calc-alkaline granitoids. *Geology* **1997**, *25*, 743–746.

73. Keskin, M. FC-modeler: A Microsoft® Excel© spreadsheet program for modeling Rayleigh fractionation vectors in closed magmatic systems. *Comput. Geosci.* **2002**, *28*, 919–928. [CrossRef]

74. Bailey, D.K. Volcanism, Earth Degassing and Replenished Lithosphere Mantle. *Philos. Trans. R. Soc. Lond. A Math. Phys. Eng. Sci.* **1980**, *297*, 309–322. [CrossRef]

75. Seddik, A.M.A.; Darwish, M.H.; Azer, M.K.; Asimow, P.D. Assessment of magmatic versus post-magmatic processes in the Mueilha rare-metal granite, Eastern Desert of Egypt, Arabian-Nubian Shield. *Lithos* **2020**, *366–367*, 105542. [CrossRef]

76. Sami, M.; Azer, M.; Abdel-Karim, A.-A. Postcollisional Ferani Volcanics from North Arabian–Nubian Shield (South Sinai, Egypt): Petrogenesis and Implication for Ediacaran (607–593 Ma) Geodynamic Evolution. *J. Geol.* **2022**, *130*, 475–498. [CrossRef]

77. Irber, W. The lanthanide tetrad effect and its correlation with K/Rb, Eu/Eu∗, Sr/Eu, Y/Ho, and Zr/Hf of evolving peraluminous granite suites. *Geochim. Et Cosmochim. Acta* **1999**, *63*, 489–508. [CrossRef]

78. Bau, M. Controls on the fractionation of isovalent trace elements in magmatic and aqueous systems: Evidence from Y/Ho, Zr/Hf, and lanthanide tetrad effect. *Contrib. Mineral. Petrol.* **1996**, *123*, 323–333. [CrossRef]

79. Jahn, B.-m.; Wu, F.; Capdevila, R.; Martineau, F.; Zhao, Z.; Wang, Y. Highly evolved juvenile granites with tetrad REE patterns: The Woduhe and Baerzhe granites from the Great Xing'an Mountains in NE China. *Lithos* **2001**, *59*, 171–198. [CrossRef]

80. Monecke, T.; Kempf, U.; Monecke, J.; Sala, M.; Wolf, D. Tetrad effect in rare earth element distribution patterns: A method of quantification with application to rock and mineral samples from granite-related rare metal deposits. *Geochim. Et Cosmochim. Acta* **2002**, *66*, 1185–1196. [CrossRef]

81. London, D.; Morgan, G.B.; Babb, H.A.; Loomis, J.L. Behavior and effects of phosphorus in the system Na_2O–K_2O–Al_2O_3–SiO_2–P_2O_5–H_2O at 200 MPa(H_2O). *Contrib. Mineral. Petrol.* **1993**, *113*, 450–465. [CrossRef]

82. Collins, W.J.; Beams, S.D.; White, A.J.R.; Chappell, B.W. Nature and origin of A-type granites with particular reference to southeastern Australia. *Contrib. Mineral. Petrol.* **1982**, *80*, 189–200. [CrossRef]